frontiers in Earth Science

ORIGINAL RESEARCH
published: 15 January 2021
doi: 10.3389/feart.2020.599388

Short-Term Monitoring of Geogenic Soil CO_2 Flux in a Non-Volcanic and Seismically Inactive Emission Site, South Korea

Chan Yeong Kim[1†], *Soonyoung Yu*[2*], *Yun-Yeong Oh*[2†], *Gitak Chae*[1], *Seong-Taek Yun*[2] *and Young Jae Shinn*[1]

[1]Korea Institute of Geoscience and Mineral Resources (KIGAM), Daejeon, South Korea, [2]Department of Earth and Environmental Sciences and Korea-CO2 Storage Environmental Management (K-COSEM) Research Center, Korea University, Seoul, South Korea

Temporal changes of soil CO_2 flux (FCO_2) and soil CO_2 concentration ($[CO_2]_v$) were surveyed in a natural CO_2 emission site to characterize the factors controlling the short-term temporal variation of geogenic FCO_2 in a non-volcanic and seismically inactive area. Due to a lack of long-term monitoring system, FCO_2 was discontinuously measured for three periods: I, II at a high FCO_2 point (M17) and III about 30 cm away. Whereas $[CO_2]_v$ was investigated at a point (60 cm depth) for all periods. A 2.1 magnitude earthquake occurred 7.8 km away and 20 km deep approximately 12 h before the period II. The negative correlation of FCO_2 with air pressure suggested the non-negligible advective transport of soil CO_2. However, FCO_2 was significantly and positively related with air temperature as well, and $[CO_2]_v$ showed different temporal changes from FCO_2. These results indicate the diffusive transport of soil CO_2 dominant in the vadose zone, while the advection near the surface. Meanwhile $[CO_2]_v$ rapidly decreased while an anomalous FCO_2 peak was observed during the period II, and the CO_2 emission enhanced by the earthquake was discussed as a possible reason for the synchronous decrease in $[CO_2]_v$ and increase in FCO_2. In contrast, $[CO_2]_v$ increased to 56.8% during the period III probably due to low gas diffusion at cold weather. In addition, FCO_2 was low during the period III and showed different correlations with measurements compared to FCO_2 at M17, implying heterogeneous CO_2 transport conditions at the centimeter scale. The abnormal FCO_2 observed after the earthquake in a seismically inactive area implies that the global natural CO_2 emission may be higher than the previous estimation. The study result suggests a permanent FCO_2 monitoring station in tectonically stable regions to confirm the impact of geogenic CO_2 to climate change and its relation with earthquakes.

Keywords: geogenic soil CO_2 flux, temporal changes, controlling factors, non-volcanic and seismically inactive, earthquake

OPEN ACCESS

Edited by:
Guodong Zheng,
Chinese Academy of Sciences (CAS), China

Reviewed by:
Jianguo Du,
China Earthquake Administration, China
Zhi Chen,
China Earthquake Administration, China
Georgy Alekseevich Chelnokov,
Geological Institute (RAS), Russia

****Correspondence:***
Soonyoung Yu
iamysy@korea.ac.kr

†Present address:
Chan Yeong Kim,
Pohang Accelerator Laboratory, Pohang, South Korea
Yun-Yeong Oh,
Korea National Institute of Environmental Research, Incheon, South Korea

Specialty section:
This article was submitted to Geochemistry, a section of the journal Frontiers in Earth Science

Received: *27 August 2020*
Accepted: *26 November 2020*
Published: *15 January 2021*

Citation:
Kim CY, Yu S, Oh Y-Y, Chae G, Yun S-T and Shinn YJ (2021) Short-Term Monitoring of Geogenic Soil CO_2 Flux in a Non-Volcanic and Seismically Inactive Emission Site, South Korea. Front. Earth Sci. 8:599388. doi: 10.3389/feart.2020.599388

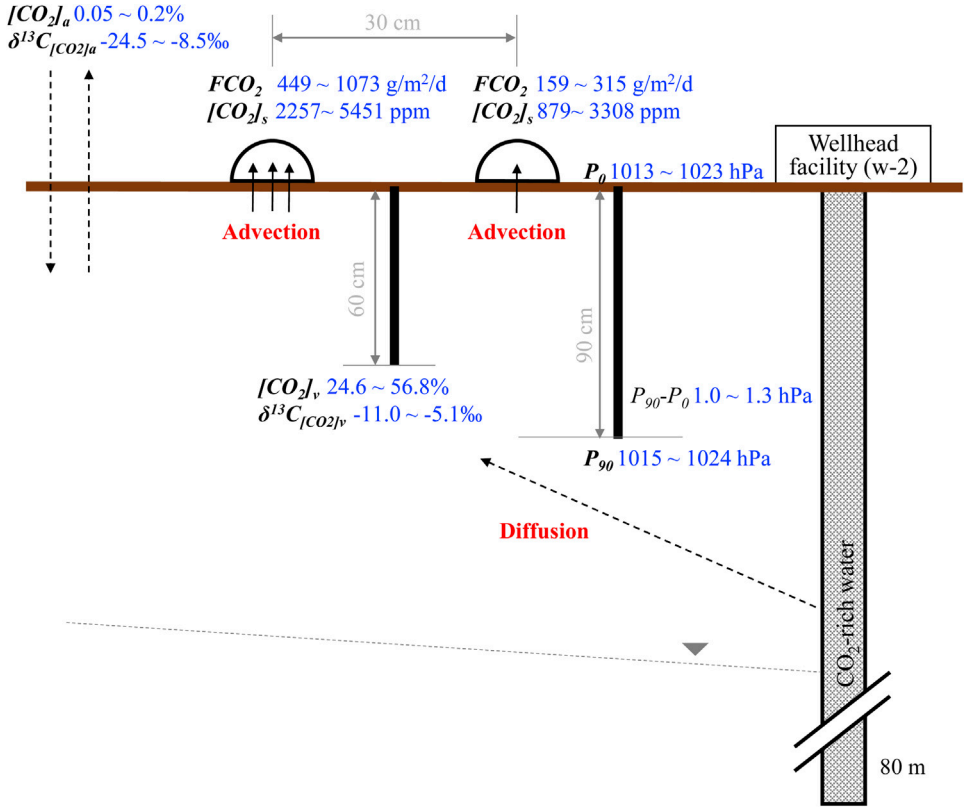

GRAPHICAL ABSTRACT |

INTRODUCTION

Annual CO_2 emission from the Earth was estimated to be approximately 600 million tonnes, with almost half produced from subaerial volcanism and the other half from non-volcanic inorganic degassing such as tectonic activities (Kerrick et al., 1995; Mörner and Etiope, 2002; Chiodini et al., 2005; Burton et al., 2013; Fischer et al., 2019). Lots of studies have been performed on the spatial distributions of geogenic soil CO_2 flux (FCO_2) for various purposes: to identify the extent of anomalous CO_2 outflow and its relation to the structural geology (e.g., Annunziatellis et al., 2008; Ciotoli et al., 2014; Ciotoli et al., 2016; Jung et al., 2014; Ascione et al., 2018; Kim et al., 2019); to calculate the total CO_2 output (e.g., Chiodini et al., 1999; Cardellini et al., 2003; Sun et al., 2018); to investigate the origin of CO_2 (e.g., Schroder et al., 2016; Chen et al., 2020); to assess volcanic (e.g., Chiodini et al., 2001; Hernández et al., 2001; Carapezza et al., 2011; Morita et al., 2019) and seismic hazards (eg, Camarda et al., 2016; Fischer et al., 2017; Sciarra et al., 2017).

Meanwhile, the temporal changes of geogenic FCO_2 and their controlling factors were relatively less studied and mostly in volcanic or seismic areas (e.g., Chiodini et al., 1998; Granieri et al., 2003; Carapezza et al., 2011; Camarda et al., 2016; Camarda et al., 2019; Oliveira et al., 2018; Morita et al., 2019; Chen et al., 2020). Morita et al. (2019) showed that barometric pressure, air temperature, soil temperature and humidity, and wind speed were decisive variables that could explain more than half of the variations in FCO_2 at 1 km southwest of the active crater of Aso volcano, while the residuals were explained using an increase in magmatic CO_2 flux. Repeated measurements by Chiodini et al. (1998) showed that FCO_2 was governed by the change in barometric pressure, while other meteorological parameters such as rain, soil and air temperature, and humidity also influenced FCO_2 in volcanic and geothermal areas. As for seismically active regions, Kerrick and Caldeira (1993), Kerrick and Caldeira (1994), Kerrick and Caldeira (1998), and Kerrick et al. (1995) studied metamorphic CO_2 degassing, including convective hydrothermal CO_2 emission. In addition, Chiodini et al. (1999) suggested the non-volcanic CO_2 derived from mantle degassing and/or metamorphic decarbonation in Central Italy. Lee et al. (2016) estimated 4 Mt/yr of mantle-derived CO_2 released along deep faults in the Magadi–Natron Basin at the border between Kenya and Tanzania. Ascione et al. (2018) introduced anomalously high FCO_2 resulting from the combination of 1) intense CO_2 generation from magmatic bodies causing decarbonation of carbonate rocks; 2) a very thin or absent top seal overlying the carbonate reservoirs; 3) the occurrence of a dense network of active fault segments at the tip of a major crustal fault zone.

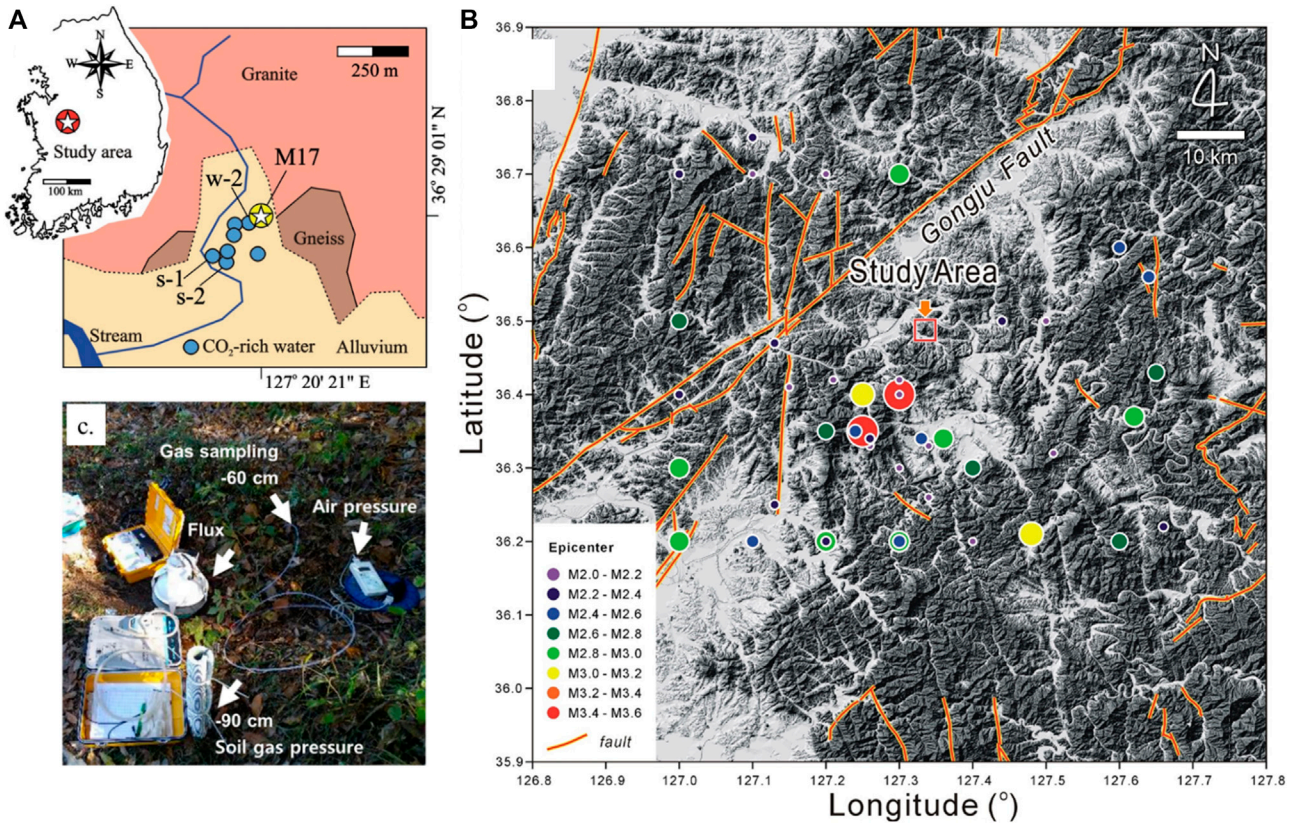

FIGURE 1 | Study area. **(A)** Location of the study point (M17) on the geological map. Five CO_2-rich groundwater wells including w-2 and two springs (s-1 and s-2) are also shown. **(B)** 49 epicenters around the study area in the past 30 years (KMA, 2019) including a recent earthquake (magnitude 2.1 and 20 km depth) occurring on November 19, 2018 at 7.8 km southwest of the study area. The larger circle indicates the larger magnitude. **(C)** Field measurements.

Moreover, seismic activity has been considered as an endogenous cause of the temporal variation of geogenic FCO_2 (Camarda et al., 2016; Camarda et al., 2019; Fischer et al., 2017; Sciarra et al., 2017; Chen et al., 2020). Specifically, Camarda et al. (2019) found that, of the two anomalous FCO_2 periods (A and C), the period A had a seismic swarm (3,471 seismic events in 79 days; Ricci et al., 2015) and thus showed the higher-amplitude anomalies than the period C. Camarda et al. (2016) showed the high spatial and temporal correlation between seismicity and FCO_2 in a district with continuous seismic activity, whereas FCO_2 varied independently in the districts with low and sporadic seismicity. According to Chen et al. (2020), seismic activity also can be responsible for the jumpily temporal variations of CO_2 concentration and flux in soil gas wells. Furthermore, vibro-stimulation was applied to increase the oil production based on the physics that the rate of degassing increases due to vibration energy (Kouznetsov et al., 1998; Kouznetsov et al., 2002).

However, studies have been rarely conducted about either the temporal variation of geogenic FCO_2 or the effect of small seismic events to FCO_2 in a geologically quiescent (e.g., non-volcanic or seismically inactive) environment. As an alternative, CO_2-rich waters have been studied in tectonically stable regions, in particular as a natural analogue study of geologic carbon storage to understand CO_2 leakage (e.g., Chae et al., 2016), because non-volcanic CO_2 is discharged by high-CO_2 groundwater as well as by focused degassing (Chiodini et al., 1999). For instance, in South Korea, which has no active volcanoes and had been relatively safe from seismic activity until the 2016 Gyeongju earthquake (M 5.8) (Woo et al., 2019), CO_2-rich waters have been studied to identify anomalously high soil CO_2 areas, and their origins (e.g., magmatic degassing, metamorphic devolatilization, oxidation of organic matter) and ascending pathways. According to Jeong et al. (2005), the CO_2 gas derived from a deep-seated source moves into the groundwater system along faults or geologic boundaries in South Korea. However, FCO_2 has been rarely studied, which motivated this study.

This study aimed 1) to characterize the temporal variation of FCO_2 in a non-volcanic and seismically inactive site (**Figure 1A**) where soil CO_2 was suggested to have a deep-seated magmatic origin (Kim et al., 2019), and 2) to identify the factors controlling the temporal changes of geogenic FCO_2. The time-variant CO_2 supply and the effect of a small earthquake were discussed. This study contributes to provide a new study direction of long-term FCO_2 monitoring to the atmosphere in tectonically stable regions,

which is important to assess due to the impacts of CO_2 on climate change, whereas many existing studies have focused on volcanic or seismic regions.

STUDY AREA

The study area (Daepyeong; Lat. 36°29′01″N and Long. 127°20′21″E) is located in the central South Korea (**Figure 1A**) and in the middle of a small basin (about 1.1 km^2). The small watershed is surrounded by mountains lower than 270 m above sea level, and the low and flat area of the basin is mostly used for rice cultivation. There are also farmhouses and gardens that cultivate vegetables, fruits, and pine saplings on a small scale.

The bedrock of the study area consists of Precambrian gneiss that was intruded by Jurassic granite (**Figure 1A**). The gneiss and granite are overlain by Quaternary sediments at lower altitudes. It is noticeable that the study area is located at the geologic boundary between gneiss and granite, along which five CO_2-rich groundwater wells and two CO_2-rich springs occur (**Figure 1A**; Jeong et al., 2001; Jeong et al., 2005; Chae et al., 2016). Chae et al. (2016) observed fractures (fissures and/or joints) and CO_2 bubbles from the fractures at a CO_2-rich spring (s-1). Kim et al. (2019) found a high FCO_2 point (M17 in **Figure 1A**) about 1.8 m away from a CO_2-rich groundwater well (w-2) to release geogenic CO_2 through the soil layer among a total of 94 points within 1 km^2. The well (w-2) has a depth of 80 m and a diameter of 150 mm, and CO_2-rich water is irregularly taken at w-2 for domestic usage by countless residents. The contact of gneiss and granite is observed on a slope near the well w-2.

A fault has not been identified in the study area (MCT et al., 2006), whereas there are faults in a regional scale including the closest Gongju Fault approximately 13 km away from the study area (**Figure 1B**). At the regional scale, the study area is located on the southwest of the NE/SW trending Ogcheon Belt (Ogcheon region). The Ogcheon Belt is a fold-and-thrust belt affected by several deformational phases, and the Ogcheon region is mainly composed of metamorphosed clastic and volcanic rocks (Kihm and Kim, 2003). In the Ogcheon region, CO_2-rich waters occur in the NE-SW direction (**Supplementary Figure S1**), parallel to the Gongju Fault and Ogcheon Belt, which implies the relation of CO_2-rich waters to faults or fractures, while no evidence has yet been found.

A total of 49 small earthquakes (≥magnitude 2.0) occurred within 30 km from the study area in the past 30 years (**Figure 1B**; KMA, 2019), including the 2.1 magnitude (M) earthquake occurring on 03:34 November 19, 2018 at 7.8 km southwest of the study area and 20 km deep. The information of focal depths is available only for five earthquakes occurring after 2017 and in the range of 11–20 km. The distribution of earthquake epicenters and their magnitudes indicate that the study area is relatively free from seismic hazards, while there may be unidentified and buried fractures.

The annual average temperature of the study area was 12.2°C, while the annual average relative humidity (*RH*) was 70.8% in 1967–2004 (MCT et al., 2006). The atmospheric temperature (T_{aws}) varied from 2.5 to 17.8°C in the period Ⅰ (**Table 1**; KMA, 2019). There was no rainfall, while it rained a week before the period Ⅰ. The total rainfall amount was 35.3 mm from October 26 to 29, 2018. During the periods Ⅱ and Ⅲ, T_{aws} ranged between −0.9 and 12.7°C and between −10.7 and 9.5°C (**Table 1**), and the total amount of precipitation was 6.5 and 1.0 mm (**Supplementary Figure S2**), respectively.

METHODOLOGY

This study was conducted around the M17 point in **Figure 1A** found by a preliminary study on the spatial variation of FCO_2 around the CO_2-rich wells and springs with 50 –100 m spacing within 1 km^2 (Kim et al., 2019). Among a total of 94 points, M17 was the only point to show geogenic CO_2 outflow through the soil layer. FCO_2 was detected up to 546 g/m^2/d, while the soil CO_2 concentration at a depth of 60 cm ($[CO_2]_v$) and its carbon isotope ($\delta^{13}C_{[CO2]v}$) were 36.0% and -5.7‰, respectively at M17 in summer, 2017 (**Table 1**), which were much higher than the values of biogenic origin (average FCO_2 of 44.9 g/m^2/d, $[CO_2]_v$ of 0.7% and $\delta^{13}C_{[CO2]v}$ of −25.2‰) observed at 79 samples in the study area (Kim et al., 2019).

Three Periods

Field works were conducted through three periods Ⅰ (from November 2 to 5, 2018), Ⅱ (November 19, 2018 to January 30, 2019), and Ⅲ (December 2 to 8, 2019) (**Table 1**; **Supplementary Figure S2**). Monitoring during the periods Ⅰ and Ⅲ was conducted to assess the background level of FCO_2 and CO_2 concentration in soil gas ($[CO_2]_v$), while FCO_2 and $[CO_2]_v$ were investigated during the period Ⅱ to assess the effect of a 2.1 M earthquake nearby (i.e., 7.8 km southwest and 20 km deep) on FCO_2.

Note that there is no long-term automated FCO_2 measurement system in the study area unlike other seismic or volcanic areas (e.g., Chiodini et al., 2001; Camarda et al., 2016; Morita et al., 2019) because FCO_2 is not a big concern. Besides, the study area is a private land. Thus, data were missing between periods, and measurement frequency varied at each period (**Supplementary Figure S2**) depending on the situations in the field (e.g., accessibility, power supply). Specifically, FCO_2 measurement and soil gas sampling were conducted simultaneously every 2 h during the period Ⅰ. Atmospheric air samples were collected in an 8-h interval approximately 1 m above the surface. Two weeks after the period Ⅰ ended, a 2.1 M earthquake occurred. Thus, further investigations for FCO_2 and soil gas were conducted since about 12 h after the earthquake occurred (period Ⅱ). FCO_2 was measured three times a day (at 14:00, 15:00, and 16:00), while soil gas samples were taken once a day (around at 14:00) until November 25. Then FCO_2 and soil gas were monitored once a week between December 26, 2018 and January 30, 2019 (**Table 1**). Lastly, FCO_2 was frequently (every 30 min) measured for a week from 00:30 December 2 to 22:30 December 8, 2019 (period Ⅲ). Soil gas and atmospheric gas samples were collected once at 15:00 on 8 December, 2019 for comparison.

TABLE 1 | Measurement results (mean ± standard deviation and range). '*n*' represents the number of measurements.

Variable[a]	Unit	Period				August, 2017 (Kim et al., 2019)
		I	II until November 25, 2018	II after December 26, 2018[b]	III	
FCO_2	g/m^2/d	564 ± 52 (*n* = 42) (449–674)	727 ± 99 (*n* = 22) (580–1,073)	606 ± 100 (*n* = 18) 449–802	228 ± 25 (*n* = 328) (159–315)	546
T_s	°C	10.1 ± 5.7 (*n* = 42) (2.3–20.7)	10.4 ± 2.5 (*n* = 22) (6.8–14.8)	8.6 ± 2.7 (*n* = 18) 4.1–12.5	0.0 ± 4.7 (*n* = 329) (–9.3–14.9)	25.5
RH_s	%	83 ± 16 (*n* = 43) (25–97)	78 ± 10 (*n* = 22) (59–95)	50 ± 12 (*n* = 18) 38–73	68 ± 17 (*n* = 329) (18–95)	89.0
$[H_2O]_s$	mmol/mol	10.4 ± 2.3 (*n* = 42) (6.9–14.5)	9.9 ± 1.6 (*n* = 22) (7.4–12.4)	5.8 ± 1.7 (*n* = 18) 3.3–8.3	4.3 ± 1.5 (*n* = 329) (1.6–8.4)	29.6
$[CO_2]_s$	ppm	3,271 ± 500 (*n* = 42) (2,457–5,451)	3,504 ± 410 (*n* = 22) (2,697–4,272)	2,926 ± 404 (*n* = 18) (2,257–3,643)	1,423 ± 484 (*n* = 329) (879–3,308)	4,428
P_s	hPa	999 ± 2 (*n* = 42) (996–1,005)	999 ± 2 (*n* = 22) (996–1,003)	999 ± 4 (*n* = 18) 994–1,006	1,002 ± 5 (*n* = 329) (992–1,011)	987
P_{aws}	hPa	1,025 ± 2 (*n* = 43) (1,021–1,030)	1,024 ± 2 (*n* = 22) (1,021–1,028)	1,025 ± 4 (*n* = 18) 1,020–1,033	1,030 ± 5 (*n* = 333) (1,019–1,039)	1,013
T_{aws}	°C	9.7 ± 5.0 (*n* = 43) (2.5–17.8)	8.0 ± 2.9 (*n* = 22) (4.0–12.7)	3.7 ± 3.6 (*n* = 18) –0.9–8.1	–0.3 ± 4.2 (*n* = 333) (–10.7–9.5)	25.1
RH_{aws}	%	65 ± 23 (*n* = 43) (25–96)	48 ± 25 (*n* = 22) (17–94)	28 ± 5 (*n* = 18) 22–37	68 ± 20 (*n* = 333) (23–100)	68
WS_1	m/s	0.7 ± 0.5 (*n* = 43) (0.0–2.3)	1.5 ± 1.0 (*n* = 22) (0.1–4.2)	2.1 ± 0.9 (*n* = 18) 0.6–3.9	1.3 ± 1.1 (*n* = 328) (0.0–7.6)	1
WS_{10}	m/s	0.7 ± 0.4 (*n* = 43) (0.0–1.9)	1.4 ± 0.8 (*n* = 22) (0.4–3.0)	1.9 ± 0.8 (*n* = 18) 0.9–3.5	-	1
P_0	hPa	1,017 ± 2 (*n* = 43) (1,013–1,023)	-	-	-	
P_{90}	hPa	1,018 ± 2 (*n* = 35)[c] (1,015–1,024)	-	-	-	
ΔP	hPa	1.1 ± 0.1 (*n* = 35)[c] (1.0–1.3)	-	-	-	
$[N_2]_v$	%	42.9 ± 1.4 (*n* = 43) (40.0–46.3)	56.1 ± 0.6 (*n* = 7) (55.0–56.8)	51.5 ± 0.9 (*n* = 5) 50.6–52.9	30.3 (*n* = 1)	49.8
$[O_2]_v$	%	11.4 ± 0.3 (*n* = 43) (10.6–12.2)	14.9 ± 0.2 (*n* = 7) (14.7–15.1)	13.6 ± 0.1(*n* = 5) 13.4–13.8	7.8 (*n* = 1)	13.2
$[CO_2]_v$	%	43.8 ± 1.9 (*n* = 43) (39.6–48.9)	26.1 ± 1.0 (*n* = 7) (24.6–27.3)	32.5 ± 0.9 (*n* = 5) 31.0–33.2	56.8 (*n* = 1)	36.0
$[N_2]_a$	%	77.9 ± 0.8 (*n* = 11) (76.9–79.0)	-	-	76.6 (*n* = 1)	20.8
$[O_2]_a$	%	20.6 ± 0.1 (*n* = 11) (20.5–20.7)	-	-	20.4 (*n* = 1)	77.3
$[CO_2]_a$	%	0.11 ± 0.05 (*n* = 9) (0.05–0.19)	-	-	0.2 (*n* = 1)	0.05
$\delta^{13}C_{[CO2]v}$	‰	–7.1 ± 1.2 (*n* = 43) (–10.1 ~ –5.4)	–7.0 ± 1.9 (*n* = 7) (–11.0 ~ –5.1)	–5.9 ± 0.5 (*n* = 5) (–6.4 ~ –5.1)	–6.2 (*n* = 1)	–5.7
$\delta^{13}C_{[CO2]a}$	‰	–19.0 ± 2.8 (*n* = 10) (–24.5 ~ –15.7)			–8.5 (*n* = 1)	–10.6

[a]*See* ***Supplementary Table S1*** *for details.*

[b]*weekly monitored.*

[c]P_{90} *values (thus* $\Delta P = P_{90}$-P_0*) were missing between 8 PM on November 2 and 10 AM on November 3 (see* ***Figure 3****).*

The FCO_2 measurement point during the period III was not exactly the same as M17, and about 30 cm away from M17 (called M17–1 hereafter) because the flux measurement device (i.e., LI-COR) had to be reinstalled in December, 2019 and we did not expect that the small spatial distance (i.e., 30 cm separation) affected the FCO_2 measurement. In contrast, $[CO_2]_v$ was investigated from the same tube (M17v) installed in August 2017 by Kim et al. (2019) for all three periods.

Sampling and Measurement

FCO_2, compositions of soil gas and atmospheric air, and their stable carbon isotopes ($\delta^{13}C_{CO2}$) were monitored. In addition, gas pressures were measured at a depth of 90 cm (P_{90}) and on the surface (P_0) during the period I. Meteorological parameters were obtained from an automatic weather station (AWS) of the Korea Meteorological Administration (KMA) near the study area (about 10 km away). All the measurements and their devices were summarized in **Supplementary Table S1**. FCO_2, P_0, and P_{90} measurements (*CO_2 flux and Gas Pressure Measurement*) and gas sampling and analysis (*Ga Sampling and Analysis*) were detailed below.

CO_2 flux and Gas Pressure Measurement

A PVC collar (height of 11.5 cm and inside diameter of about 20 cm) was implanted into the soil, on which a bottom-opened chamber was placed (**Figure 1C**). Then pressure (P_s; hPa), temperature (T_s; °C), relative humidity (RH_s; %), CO_2 concentration ($[CO_2]_s$; ppm), and water vapor mole fraction ($[H_2O]_s$; mmol/mol) in the soil chamber were measured for 2 min by a built-in infrared gas analyzer using LI-COR 8100A (LI-COR Inc. Lincoln, NE, USA). FCO_2 (g/m^2/d) was calculated by **Equation 1** as Jung et al. (2014):

$$FCO_2 = k\frac{10V\,P\left(1-\frac{[H_2O]}{1000}\right)}{R\cdot S(T+273.15)}\frac{d[CO_2]}{dt} \quad (1)$$

where k is a unit conversion factor (3.80 g·s/μmol/d), R is the universal gas constant (8.31 m^3·Pa/K/mol), S is the soil surface area (herein, 317.8 cm^2 for the about 20 cm diameter chamber), V is the system volume (i.e., the sum of the chamber volume and the extra volume by a offset), P, T, and $[H_2O]$ are the initial P_s, T_s, and $[H_2O]_s$, respectively, and $d[CO_2]/dt$ is the rate of change in $[CO_2]_s$ for the 2-min measurement.

Pore gas pressure (P_{90}) and atmospheric pressure (P_0) were monitored using a pressure transducer (BAT® geosystem). A porous filter tip was connected to the end of a 2.54 cm diameter pipe and then installed to a target depth (i.e., 90 cm). Then the pressure transducer with a needle was poked to the rubber on the top of the filter tip. Pressures were measured at a 1-min interval over the whole survey period I. However, 30-min average values

of P_{90} and P_0 were used when the relationships with other measurements were assessed. In other words, P_{90} and P_0 data (thus $\Delta P = P_{90} - P_0$) were taken for 15 min before and after the FCO_2 measurement, respectively and then averaged for the 30 min.

Ga Sampling and Analysis

Soil gas samples were taken using a Teflon tube which had the outer diameter of 0.64 cm and was embedded down to 60 cm below the surface with the AMS Gas Vapor Probe (AMS, Inc., USA). Atmospheric air samples were collected 1 m above the surface. Soil gas and atmospheric air samples were purged for 5 min using a portable Masterflex E/S peristaltic pump (Cole-Parmer Instruments, USA) and then collected in a 1 L multi-layered Tedlar bag (Restek©, USA). Soil gas duplicates were collected once a day (at 14:00; n = 4) during the period I to double check the results of $\delta^{13}C_{[CO2]v}$ analysis, with connecting the y-shaped adapter at the end of the sampling tube.

The carbon isotope of CO_2 ($\delta^{13}C_{CO2}$) in the gas samples were analyzed by the Picarro G2121-i isotope and gas analyzer (Picarro Inc., USA) at the Korea Institute of Geoscience and Mineral Resources (KIGAM). The Picarro cavity ring-down spectroscopy (CRDS) was calibrated by IAEA standard materials ($\delta^{13}C_{CO2}$ = 2.492, −5.764, −47.321‰) before analyzing samples. All gas samples were purged for 10 min with laboratory air and then analyzed for 15 min to avoid the memory effect. Results were expressed relative to the international V-PDB standard. The soil gas duplicates (n = 4) obtained during the period I and a soil gas sample obtained during the period III were analyzed by Thermo Fisher Delta V™ IRMS (isotope ratio mass spectrometer) at Beta Analytic Inc. (Miami, USA) for comparison.

Gas compositions (N_2, O_2, and CO_2) were determined by the Agilent 490 Micro Gas Chromatograph (GC) at KIGAM. Before the laboratory analysis, two columns in GC (i.e., CP-Molsieve 5A column for N_2 and O_2 and PoraPLOT U column for CO_2) were calibrated by three different standards (CO_2 = 49.98; 5.00; 0.04%: Rigas©, Korea). Each sample was analyzed at least three times, and the coefficient of variation was less than 0.9% for CO_2.

Statistical Analysis and CO_2 Solubility Calculation

Simple statistical analyses were applied for each period because of discontinuous and short-term observations at different intervals. First, Pearson correlation coefficients (r) were calculated to evaluate the effect of environmental parameters to FCO_2, and to find the relation varying depending on a measurement period. According to Camarda et al. (2019), the response of FCO_2 to exogenous parameter variations is dependent on the predominant process of CO_2 transport through the soil. At sites with diffusion-dominated CO_2 transport, FCO_2 was mainly affected by variation in the volumetric water content of the soil and the air temperature, while at sites with high fluxes and non-negligible advective components, FCO_2 was affected solely by variation in the atmospheric pressure (Camarda et al., 2019). The relationship between FCO_2 and exogenous parameters is also influenced by the amount of deep CO_2 supply. Then multiple regression was used to explain the relationship between FCO_2 and highly correlated environmental parameters and to estimate the effect of endogenous parameters. Regression analyses have been widely conducted (Granieri et al., 2003; Vodnik et al., 2009; Carapezza et al., 2011; Camarda et al., 2016; Oliveira et al., 2018; Morita et al., 2019) to distinguish the effect of each factor to the FCO_2 variation, including endogenous (e.g., seismicity) and environmental parameters. It should be noted that we used P_s, T_s, $[CO_2]_s$ and $[H_2O]_s$ in the soil chamber measured for 2 min using LI-COR 8100A as environmental parameters (see **Table 1** and **Supplementary Table S1**) and discussed their usefulness (*Environmental Parameters*), because they represent the mixture of soil efflux from the soil layer for 2 min and the air initially filling the chamber, and are different from the initial values used to calculate FCO_2 in **Equation 1**.

Second, autocorrelation of time series was assessed to find the periodicity for the data obtained during the periods I and III (**Supplementary Figures S3, S4**). Cross-correlation coefficients (R_{xy}) were evaluated for the data obtained during the period I to characterize the lead-lag relationship between input variables (x; measurements in **Table 1**) and output variables (y; mainly FCO_2 in this study) and a time lag (**Supplementary Figure S5**):

$$R_{xy}\left(t_{lag}\right) = \frac{C_{xy}\left(t_{lag}\right)}{\sigma_x\left(t_{lag}\right)\sigma_y\left(t_{lag}\right)} \quad (2)$$

where C_{xy} is the covariance between x and y, while σ_x and σ_y are the standard deviations of x and y in a lag time (t_{lag}), respectively. When t_{lag}= 0, $r = R_{xy}(0)$. R statistical software was used for autocorrelation and cross-correlation analysis (R core team, 2019).

In addition, the amount of CO_2 degassing from a CO_2-rich aquifer was estimated by calculating the variation in CO_2 solubility in groundwater due to the variation in pressure, salinity and temperature based on the method by Duan and Sun (2003).

RESULTS

Background Levels

Measurements during the periods I and III were compared to assess the background levels of FCO_2 and soil gas compositions (**Table 1**) and their relations with environmental variables (**Tables 2**, **3**). **Table 4** showed R_{xy} with a non-zero t_{lag}. The other parameters showed a t_{lag} of zero with FCO_2, and thus R_{xy} = r in **Table 2** when $y = FCO_2$.

CO_2 Flux

The average FCO_2 during the period I was 564 g/m^2/d and ranged from 449 to 674 g/m^2/d, which was similar to 546 g/m^2/d obtained at M17 in August 2017 (**Table 1**) and quite high compared to FCO_2 in the other 93 points (7.5–118 g/m^2/d) in the study area measured by Kim et al. (2019) and in typical normal soil systems (~40 g/m^2/d) suggested in Ascione et al. (2018). Meanwhile, FCO_2 during the period III ranged between 159 and 315 g/m^2/d (average of 228 g/m^2/d), which was higher than those in the 93 points of Kim et al. (2019) and in typical normal soil systems by Ascione et al. (2018), but much lower than

TABLE 2 | Pearson correlation coefficients during the period I. Absolute values ≥0.6 are in bold.

	FCO_2	T_s	RH_s	$[H_2O]s$	$[CO_2]_s$	P_s	P_{awa}	T_{aws}	RH_{aws}	WS_1	WS_{10}	P_0	P_{90}	ΔP	$[N_2]_v$	$[O_2]_v$	$[CO_2]_v$	$[N_2]_a$	$[O_2]_a$	$[CO_2]_a$	$\delta^{13}C_{[CO2]v}$	$\delta^{13}C_{[CO2]a}$
FCO_2	1.0																					
T_s	0.5	1.0																				
RH_s	**−0.6**	**−0.9**	1.0																			
$[H_2O]_s$	0.5	**1.0**	**−0.8**	1.0																		
$[CO_2]_s$	0.3	0.2	−0.1	0.3	1.0																	
P_s	**−0.8**	−0.3	0.3	−0.3	−0.2	1.0																
P_{aws}	**−0.8**	−0.4	0.3	−0.3	−0.2	1.0	1.0															
T_{aws}	0.5	***1.0***	***−0.8***	**1.0**	0.3	−0.3	−0.4	1.0														
RH_{aws}	−0.4	**−0.9**	**0.7**	**−0.9**	−0.2	0.3	0.4	**−0.9**	1.0													
WS_1	0.2	**0.6**	−0.5	0.5	0.0	0.0	−0.1	**0.6**	**−0.6**	1.0												
WS_{10}	0.1	0.5	−0.4	0.5	0.0	0.1	0.1	0.5	**−0.6**	**0.8**	1.0											
P_0	**−0.8**	−0.3	0.3	−0.3	−0.2	**1.0**	**1.0**	−0.4	0.3	−0.1	0.1	1.0										
P_{90}	**−0.6**	−0.1	0.1	−0.1	−0.4	**1.0**	**1.0**	−0.1	0.1	0.2	0.4	**1.0**	1.0									
ΔP	0.4	**0.9**	**−0.8**	**1.0**	0.2	−0.2	−0.2	**0.9**	**−0.8**	0.5	0.4	−0.2	−0.1	1.0								
$[N_2]_v$	0.1	0.3	−0.3	0.3	0.1	0.1	0.0	0.4	−0.5	0.4	0.4	0.0	**0.7**	0.1	1.0							
$[O_2]_v$	0.1	0.3	−0.2	0.3	0.1	0.1	0.0	0.4	−0.5	0.4	0.4	0.0	**0.7**	0.0	**1.0**	1.0						
$[CO_2]_v$	−0.2	−0.4	0.3	−0.4	0.0	0.0	0.1	−0.4	0.5	−0.4	−0.4	0.1	**−0.6**	−0.1	**−0.9**	**−1.0**	1.0					
$[N_2]_a$	**0.6**	0.0	−0.1	−0.1	0.1	−0.5	−0.5	−0.1	0.0	−0.2	0.0	−0.5	−0.4	−0.3	−0.2	−0.3	0.1	1.0				
$[O_2]_a$	**0.9**	0.3	−0.3	0.2	0.2	**−0.8**	**−0.8**	0.3	−0.2	−0.2	−0.3	**−0.8**	**−0.8**	0.0	−0.2	−0.2	0.0	**0.7**	1.0			
$[CO_2]_a$	**−0.8**	0.0	0.0	0.0	0.0	**0.8**	**0.8**	−0.1	0.0	0.2	**0.6**	**0.8**	**0.8**	−0.1	**0.6**	**0.6**	−0.5	−0.1	**−0.7**	1.0		
$\delta^{13}C_{[CO2]v}$	−0.2	0.3	−0.2	0.2	0.0	0.2	0.2	0.3	-0.3	0.1	0.1	0.2	0.1	0.4	0.2	0.2	−0.1	−0.5	−0.5	0.4	1.0	
$\delta^{13}C_{[CO2]a}$	−0.–4	−0.2	0.1	−0.3	0.0	0.4	0.4	−0.2	0.0	−0.1	0.2	0.4	0.2	0.1	−0.2	−0.3	0.3	0.3	−0.3	**0.7**	−0.1	1.0

TABLE 3 | Pearson correlation coefficients during the period III. Absolute values ≥0.6 are in bold.

	FCO_2	T_s	RH_s	$[H_2O]_s$	$[CO_2]_s$	P_s	P_{aws}	T_{aws}	RH_{aws}	WS
FCO_2	1.0									
T_s	**0.6**	1.0								
RH_s	0.0	−0.3	1.0							
$[H_2O]_s$	0.5	**0.6**	0.5	1.0						
$[CO_2]_s$	**0.0**	−0.2	0.4	0.1	1.0					
P_s	**−0.6**	−0.4	−0.3	−0.6	−0.2	1.0				
P_{aws}	**−0.7**	−0.5	−0.3	**−0.7**	−0.2	**1.0**	1.0			
T_{aws}	**0.6**	**0.9**	−0.1	**0.7**	−0.1	−0.5	**−0.6**	1.0		
RH_{aws}	0.1	−0.2	**0.7**	0.4	0.5	−0.4	−0.4	−0.2	1.0	
WS	0.1	0.5	−0.4	0.1	−0.4	0.0	0.0	0.4	−0.5	1.0

TABLE 4 | Cross-correlation coefficients with a non-zero time lag during the period I. See **Supplementary Figure S5** for cross-correlation functions.

X	$Rx_{-,\ FCO2}$	*Time lag (*tlag*; hours)*
$[CO_2]_s$	0.3	22
WS_1	−0.4	−18
WS_{10}	−0.4	−18
ΔP	−0.5	6
$[N_2]_v$	−0.4	−14
$[O_2]_v$	−0.4	−16
$[CO_2]_v$	0.5	−16
$\delta^{13}C_{[CO2]v}$	−0.4	−14
$\delta^{13}C_{[CO2]a}$	−0.5	6

those during the period I in 2018 and that in August, 2017 (**Table 1**). $[H_2O]_s$ and $[CO_2]_s$ were also lower than those during the period I (**Table 1**; **Figure 2**). Besides, during the period I, T_s, 1/RH_s, $[H_2O]_s$, and ΔP increased daytime and decreased at night (**Figures 2**, **3** and **Supplementary Figure S3**), while the diurnal variation of $[H_2O]_s$ was not clear during the period III (**Figure 2D** and **Supplementary Figure S4**), especially until December 6, 2019 when the temperature was lowered down to −10°C and the pressure exceeded 1,010 hPa (**Figures 2B,F**). RH_s ($r = -0.6$) and RH_{aws} ($r = -0.4$) were negatively correlated with FCO_2 during the period I (**Table 2**), but not related with FCO_2 during the period III (**Table 3**).

Despite the different ranges in FCO_2 at each period, FCO_2 had significant correlations with T_s, $[H_2O]_s$, T_{aws}, P_s and P_{aws} at both periods (**Tables 2**, **3**). FCO_2 increased with increasing $[H_2O]_s$, T_s and T_{aws} but decreased with P_s and P_{aws}. In addition, P_0 and P_{90} were negatively correlated with FCO_2 during the period I. The negative relation of FCO_2 with P_{aws} was explained by the fact that a decrease in barometric pressure increases the pressure gradient of the ground, which subsequently enhances the viscous gas flux (Rogie et al., 2001; Granieri et al., 2003; Morita et al., 2019). The positive relation with T_{aws} on the short time scale was explained as the effect of variations in soil gas diffusivity with air temperature as well as surficial biological productivity (Camarda et al., 2016 and references therein). The positive effect of $[H_2O]_s$ can be explained by its positive relationship with T_s and T_{aws} and negative with P_s and P_{aws} in **Tables 2**, **3**, and will be further discussed in *Environmental Parameters* regarding the usefulness of the environmental parameters obtained in the chamber.

Soil Gas and Air

CO_2 concentrations in the soil gas obtained at a depth of 60 cm ($[CO_2]_v$) ranged from 39.6 to 48.9% (average = 43.8%) during the period I (**Figure 4A**), which were slightly higher than that measured in August, 2017 (36.0%) but lower than that during the period III (56.8%) in **Table 1**. $\delta^{13}C_{[CO2]v}$ for the soil gas was between −10.1 and −5.4‰ (average = −7.1‰) during the period I and was −6.2‰ during the period III, which were a little lower than the value (−5.7‰) obtained in August, 2017 (**Figure 4A**; **Table 1**). However, the variations in $\delta^{13}C_{[CO2]v}$ were insignificant and the $\delta^{13}C_{[CO2]v}$ values were relatively high compared to the $\delta^{13}C_{[CO2]v}$ of biogenic origin in the study area between −32.0 and −13.0‰ (average −25.2‰) in Kim et al. (2019).

$[CO_2]_v$ did not show a distinct diurnal variation during the period I (**Figure 4A**) similar to FCO_2 and $[CO_2]_s$ that showed the pattern out of the diurnal variation during both periods I and III unlike T_s, RH_s or $[H_2O]_s$ (**Figure 2**; **Supplementary Figures S3, S4**). $[CO_2]_v$ was not linearly correlated with either FCO_2 ($r = -0.2$) or $\delta^{13}C_{[CO2]v}$ ($r = -0.1$) in **Table 2**, while positively with FCO_2 at the time lag of −16 h ($R_{xy} = 0.5$ in **Table 4**; **Supplementary Figure S5**) and negatively with $\delta^{13}C_{[CO2]v}$ ($R_{xy} = -0.3$) at the time lag of −24 h (**Supplementary Figure S5**). $[CO_2]_v$ was negatively related with P_{90} ($r = -0.6$ in **Table 2**), indicating that the high P_{90} caused $[CO_2]_v$ to decrease. The average N_2 ($[N_2]_v$) and O_2 concentrations ($[O_2]_v$) of soil gas obtained at a depth of 60 cm was different between the two periods: 42.9% (40.0–46.3%) and 11.4% (10.6–12.2%) respectively during the period I, while 30.3% and 7.8% respectively during the period III (**Figure 5**; **Table 1**), probably due to the high proportion of CO_2 during the period III.

It is noticeable that both $[CO_2]_v$ and $[CO_2]_s$ showed a rapid increase during the period I with the time lag of about 12 h. Specifically, $[CO_2]_v$ rapidly increased from 39.8 to 48.9% at 22:00 on November 2 (**Figure 4A**), while $[CO_2]_s$ increased from 0.3 to 0.5% at 10:00 on November 3 (**Figure 2C**). Consistently, the cross-correlation analysis showed that the correlation between $[CO_2]_v$ and $[CO_2]_s$ increased up to 0.55 at the time lag of -12 h in **Supplementary Figure S5** from zero in **Table 2**, and suggested the transport rate of approximately 60 cm/12 h. $[CO_2]_s$ occasionally showed rapid increases during the period III as well, in particular around December 4 (see the red arrow in **Figure 2D**), whereas $[CO_2]_v$ measurements were not available for comparison.

Meanwhile the CO_2 concentrations in the air samples ($[CO_2]_a$) measured during the periods I (0.05–0.19%) and period III (0.20%) in **Figure 4B** and **Table 1** showed high values compared to a reported atmospheric CO_2 composition (0.04%) and the value previously detected in the study site (0.05%). $[CO_2]_a$ was negatively correlated with FCO_2 ($r = -0.8$) and $[CO_2]_v$ ($r = -0.5$), but not with $[CO_2]_s$ ($r = 0.0$) during the period I (**Table 2**). $\delta^{13}C_{[CO2]a}$ for the air samples was different between two periods. The average $\delta^{13}C_{[CO2]a}$ (-19.0 ± 2.8‰; $n = 10$) during the period I was much lower

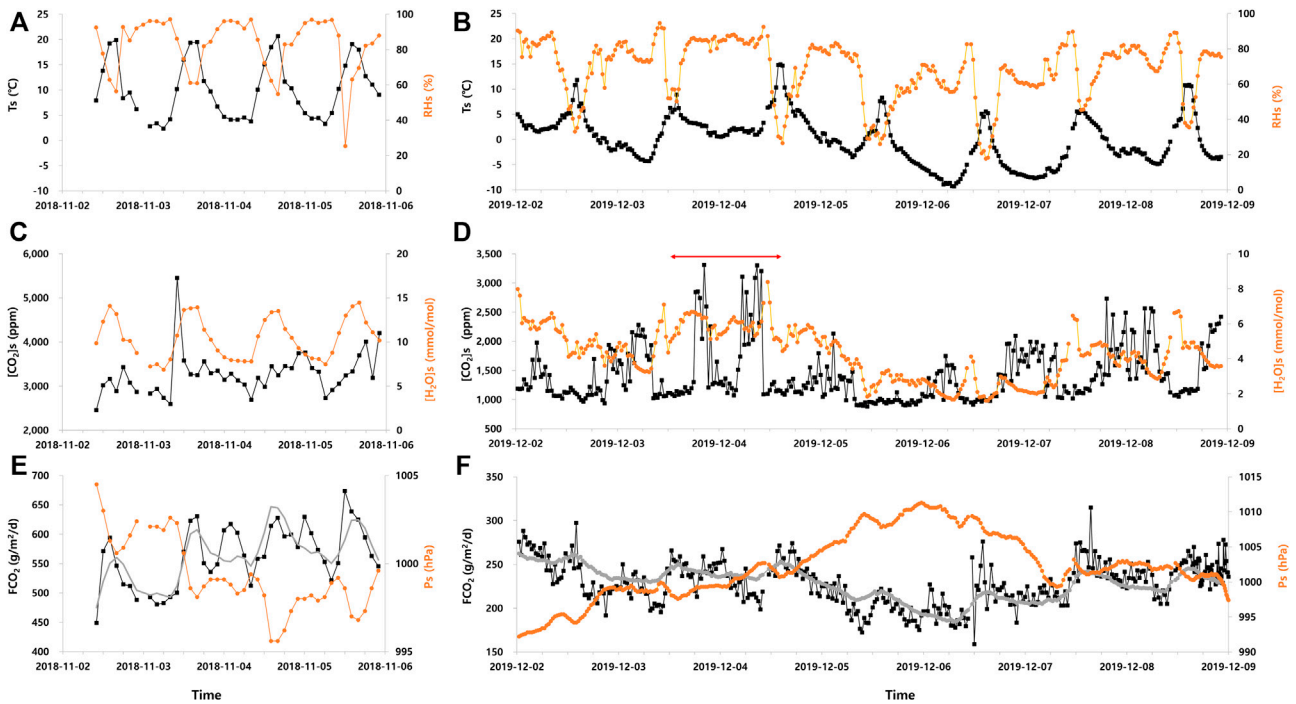

FIGURE 2 | Temporal comparison of temperature (T_s; °C), relative humidity (RH_s; %) in **(A,B)**, CO_2 concentrations ($[CO_2]_s$; ppm), water vapor mole fraction ($[H_2O]_s$; mmol/mol) in **(C,D)**, and pressure (P_s; hPa) in the chamber and calculated CO_2 flux (FCO_2; g/m^2/d) in **(E,F)** during the periods I **(left)** and III **(right)**. In **(E,F)**, the gray line addresses the FCO_2 estimated using T_{aws} and P_{aws} in **Equations 3**, **4**, respectively. Note that $[CO_2]_s$, $[H_2O]_s$, FCO_2, and P_s have different scales between two periods. The red arrow in **(D)** indicates the time of rapid increases in $[CO_2]_s$.

than the values measured during the period III (−8.5‰) and in August 2017 (−10.6‰). The higher $[CO_2]_a$, the higher $\delta^{13}C_{[CO2]a}$ (r = 0.7) during the period I. On the other hand, the air samples showed similar N_2 ($[N_2]_a$) and O_2 ($[O_2]_a$) compositions in both periods: 77.9% N_2 and 20.6% O_2 in average during the period I, while 76.6% N_2 and 20.4% O_2 during the period III. $[N_2]_a$ and $[O_2]_a$ were positively related with FCO_2 unlike $[CO_2]_a$ during the period I (**Table 2**).

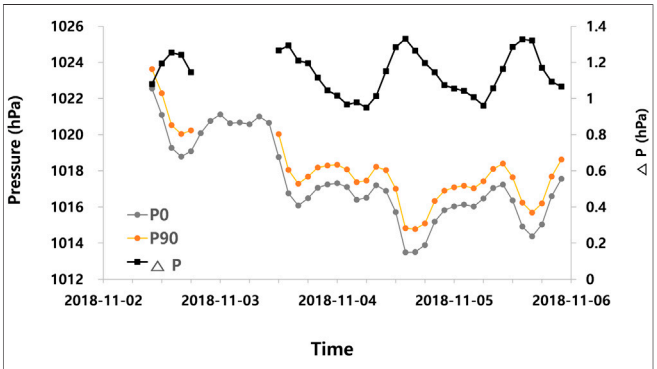

FIGURE 3 | Pressures at surface (P0; hPa) and at a depth of 90 cm (P90; hPa) measured by the BAT® geosystem and the pressure difference between P_0 and P_{90} ($\Delta P = P_{90}-P_0$; hPa) during the period I.

After the Earthquake

FCO_2 increased up to 1,073 g/m^2/d by a factor of two approximately 12 h after the earthquake (**Figure 6** and **Supplementary Figure S2**), which was much higher than the sum of mean (μ) and 2 times standard deviation (2σ) of FCO_2 during the period I (μ + 2σ; 668 g/m^2/d). Besides, relatively high FCO_2 was observed on November 25, 2018 (836 g/m^2/d) and January 23, 2019 (802 g/m^2/d) (**Figure 6**). Those high FCO_2 values were not observed either during the period I or in the previous study at M17 (**Table 1**).

The high FCO_2 seemed to be related with $[CO_2]_s$ (**Figure 7**; r = 0.9 in **Table 5**). Their high correlation was not observed in the other periods. Namely, $[CO_2]_s$ rapidly increased after the earthquake and decreased with FCO_2, and high $[CO_2]_s$ was observed on both November 25, 2018 and January 23, 2019 (**Figure 7**), although the maximum $[CO_2]_s$ (5,451 ppm) was observed during the period I (**Table 1**; **Figure 2C**). Unlike FCO_2 increasing abruptly, however, $[CO_2]_v$ dropped by about half after the earthquake, and then increased back but did not reach the pre-earthquake values until January 30, 2019, although a high value of $[CO_2]_v$ (56.8%) was observed in December, 2019 (**Table 1**). Thus, $[CO_2]_v$ was negatively related with FCO_2 during the period II (r = −0.5 in **Table 5**). The maximum $[CO_2]_s$ observed during the period I and the increasing in $[CO_2]_s$ and FCO_2 but the decreasing in $[CO_2]_v$ after the earthquake will be discussed in relation to the earthquake in *Possible Causes of a High CO_2 Emission During the Period* II.

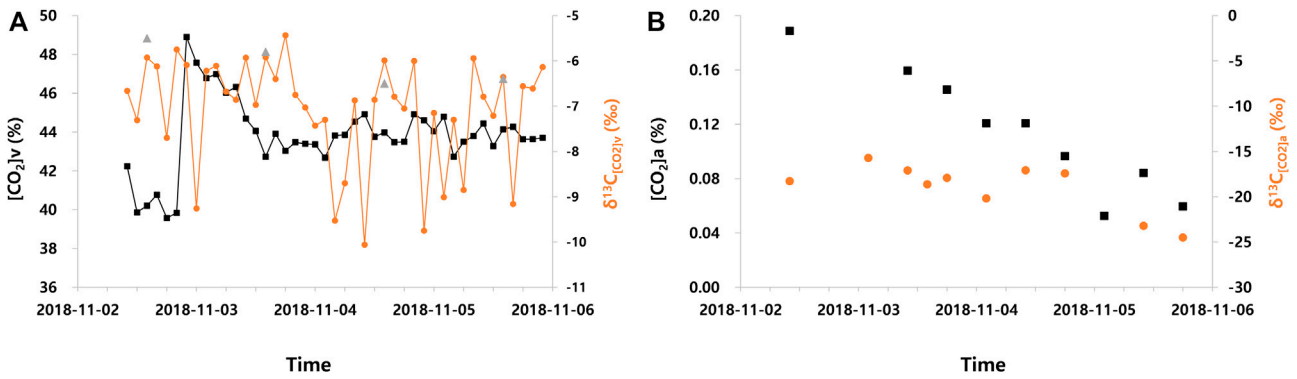

FIGURE 4 | Temporal changes of **(A)** CO_2 concentrations measured at a depth 60 cm ([CO_2]v) and its $\delta13C_{[CO2]v}$; **(B)** CO_2 concentrations in air samples ([CO_2]a) and its $\delta13C_{[CO2]a}$ during the period I. Gray triangles in **(A)** show the $\delta13C_{[CO2]v}$ values determined by the Beta Analytic Inc. (n = 4) for cross-checking.

Besides, it was observed that the relative humidity (*RH*) in the chamber (RH_s) and from the AWS (RH_{aws}) were positively related with FCO_2 during the period II (r = 0.7 and 0.4 respectively in **Table 5**) unlike the other periods, probably due to the precipitation as well as earthquake (see *Environmental Parameters*).

DISCUSSION

Source of CO_2

Scatter plots of soil gas compositions revealed that the soil gas was the mixture of atmospheric air and geogenic CO_2 (**Figure 5**). Specifically, the CO_2 vs. O_2 was plotted on the air-CO_2 mixing line (**Figure 5A**), while the N_2 vs. CO_2 was not on the biological respiration or CH_4 oxidation (**Figure 5B**). Besides, the consistent $\delta^{13}C_{[CO2]v}$ regardless of the season and the $\delta^{13}C_{[CO2]v}$ ranges (**Figure 5D**) indicated a deep-seated CO_2 source despite the different proportion of CO_2 in soil gas at each period as the $\delta^{13}C_{CO2}$ of geogenic CO_2 is reported to be −6‰ in Baines and Worden (2004) and −9.7 ~ −2.7‰ (−6.5 ± 2.5‰) in Sano and Marty (1995). In contrast, the $\delta^{13}C_{CO2}$ from the microbial decomposition of C3 plants generally ranges between −34 and −23‰ (Faure, 1998) and seasonally changes due to the change in biological activities (White and Corfield, 2006; Zhu et al., 2019). FCO_2 did not show the diurnal variation (**Supplementary Figures S2–S4**), and had a significantly negative relation with barometric pressure (**Tables 2**, **3**, **5**), which also indicates the geogenic CO_2 emission in the study site (Camarda et al., 2019). At the measurement site around M17, the geological FCO_2 seems to exceed the microbial respiratory FCO_2 by several orders of magnitude as in the sites with high CO_2 concentrations in Vodnik et al. (2009).

During the period I, P_{90} was always higher than P_0 (**Figure 3**). The positive ΔP indicates that the atmospheric air did not intrude and dilute $[CO_2]_v$ at the measurement point (M17v). Instead, the mixing with air seemed to be diffusive at M17v due to concentration gradients with depth, which may be affected by the barometric pressure given that P_{90} was synchronized with P_0 (**Figure 3**). Besides, the geogenic CO_2 uprising could be mixed with soil gas influenced by the atmospheric air in the vadose zone. According to Massmann and Farrier (1992) and Chen et al. (2020), the changes in barometric pressure migrate air into the vadose zone. Air intrusion due to the barometric pressure fluctuation depends on soil characteristics, the thickness of vadose zone, and climate (Massmann and Farrier, 1992; Auer et al., 1996).

Meanwhile, $\delta^{13}C_{[CO2]a}$ was widely ranged particularly during the period I (**Figure 4B**) probably due to various sources of CO_2 in the air 1 m above the surface. A CO_2 source in the air seemed to be geogenic given high $[CO_2]_a$ values up to 0.2% (**Table 1**), the positive relation between $[CO_2]_a$ and $\delta^{13}C_{[CO2]a}$ (r = 0.7 in **Table 2**; **Figure 4B**), and the significant relations between air compositions and FCO_2 (**Table 2**).

Factors to Control Geogenic CO_2 Flux

The variation in geogenic FCO_2 depends on soil properties (e.g., air permeability and diffusion coefficient), prevailing mechanisms of CO_2 transport (e.g., advection and diffusion), environmental parameters (e.g., air pressure and temperature), and deep-seated CO_2 supply via endogenous processes (e.g., volcano and tectonic activity). We discussed the factors controlling the temporal variations of FCO_2 in relation to time-variant geogenic CO_2 supply due to exploitation of CO_2-rich water (*Time-Variant Supply of Geogenic CO_2)*, the effect of environmental variables including precipitation (*Environmental Parameters*), and the prevailing mechanisms of CO_2 transport (*Prevailing Mechanisms of CO_2 Transport*). *Besides, the difference between the periods* I *and* III *was discussed with respect to the spatial variability of* FCO_2 (Heterogenous Transport of Geogenic CO_2). Soil properties could not be investigated in this private land.

Time-Variant Supply of Geogenic CO_2

The geogenic CO_2 supply seemed to be variant with time given the irregular increases of $[CO_2]_s$ (i.e., CO_2 concentration in the chamber 2 min after closing the chamber in **Figure 2**) regardless of environmental variables (**Tables 2**, **3**). According to Kim et al. (2019), CO_2 gas in the study area forms by degassing from the water table of a CO_2-rich aquifer

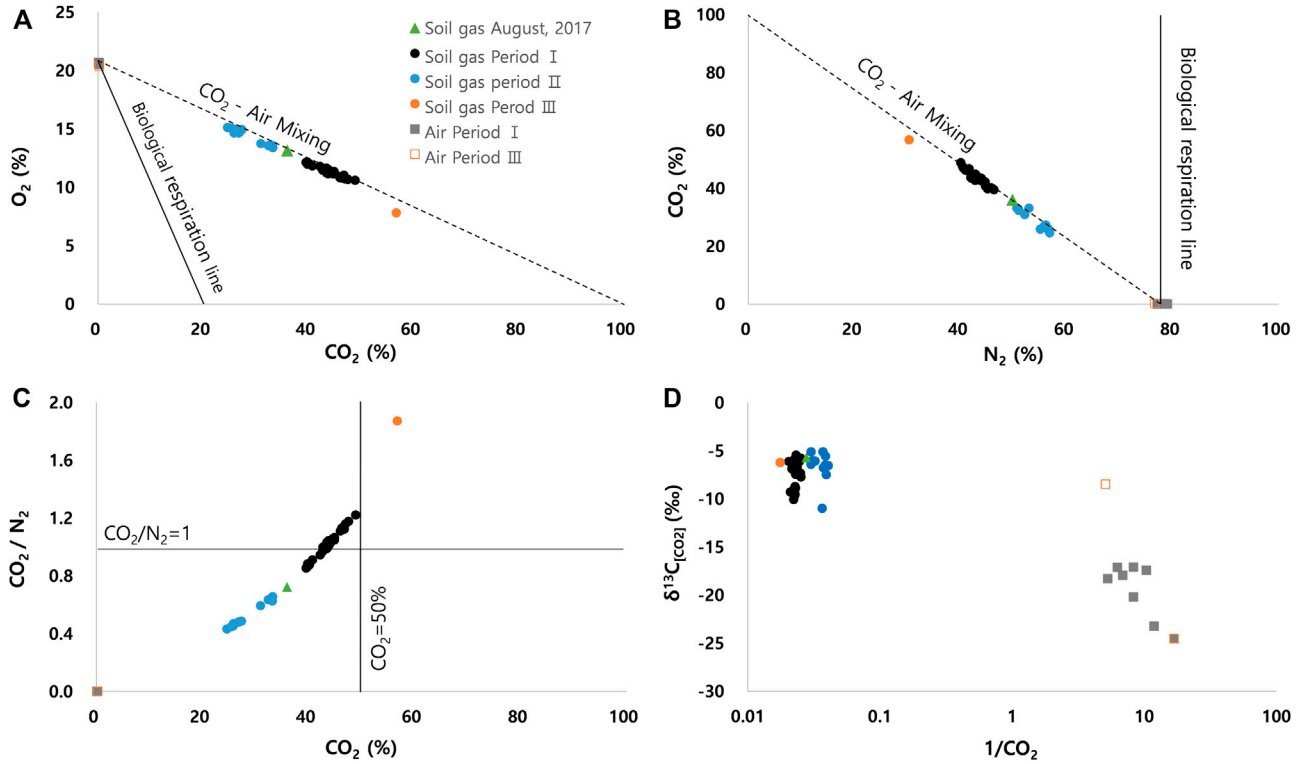

FIGURE 5 | Compositions and stable carbon isotopes ($\delta 13C_{[CO2]}$) of soil gas and atmospheric air. The relationships between CO_2 and O_2 **(A)** and between N_2 and CO_2 **(B)** (after Romanak et al., 2012). Dotted lines represent the mixing between atmospheric air concentrations measured in this study and 100% geogenic CO_2, while solid lines represent the biological respiration in **(A,B)**. **(C)** CO_2/N_2 vs. CO_2; **(D)** $1/CO_2$ vs. $\delta 13C_{[CO2]}$ (after Sun et al., 2018). The soil gas data in August 2017 is from Kim et al. (2019).

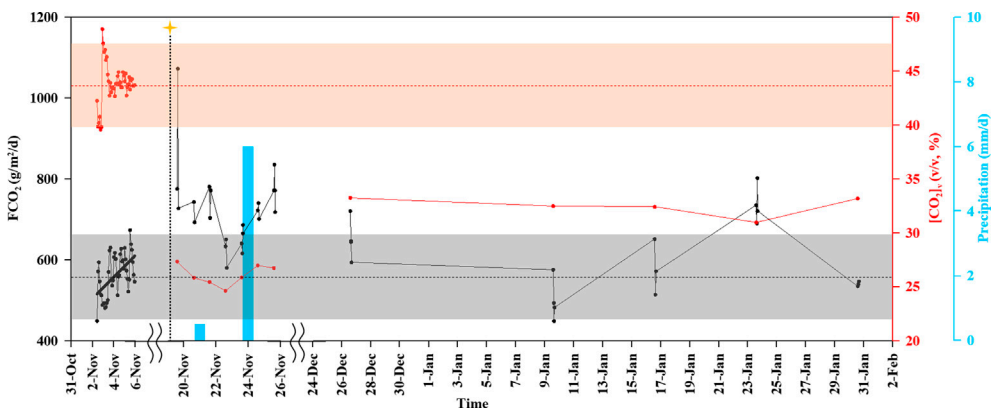

FIGURE 6 | Temporal changes of CO_2 flux (FCO_2) and CO_2 concentrations measured at a depth 60 cm ($[CO_2]v$) before and after the 2.1 M earthquake (yellow star) occurred on November 19, 2018. The shaded areas cover the mean (μ; dotted line) ± two times standard deviation (2σ) of the period Ⅰ (**Table 1**). The solid thick line represents the linear regression (r^2 = 0.3).

and transports toward the M17 site and leaks at M17 via the voids surrounding the well w-2. The amount of CO_2 degassing is expected to be time-variant because the CO_2-rich water is taken from w-2 by countless people, which changes the groundwater level and subsequently the fluid pressure, affecting the amount of CO_2 degassing (Duan and Sun, 2003). The time-variant CO_2 degassing seemed to alter $[CO_2]_v$ and the CO_2 gradient in the subsurface, and subsequently $[CO_2]_s$, for instance with the time lag of −12 h between M17v and M17(**Supplementary Figure S5E**) and consequently FCO_2 with the time lag of −16 h (**Table 4**) during the period Ⅰ.

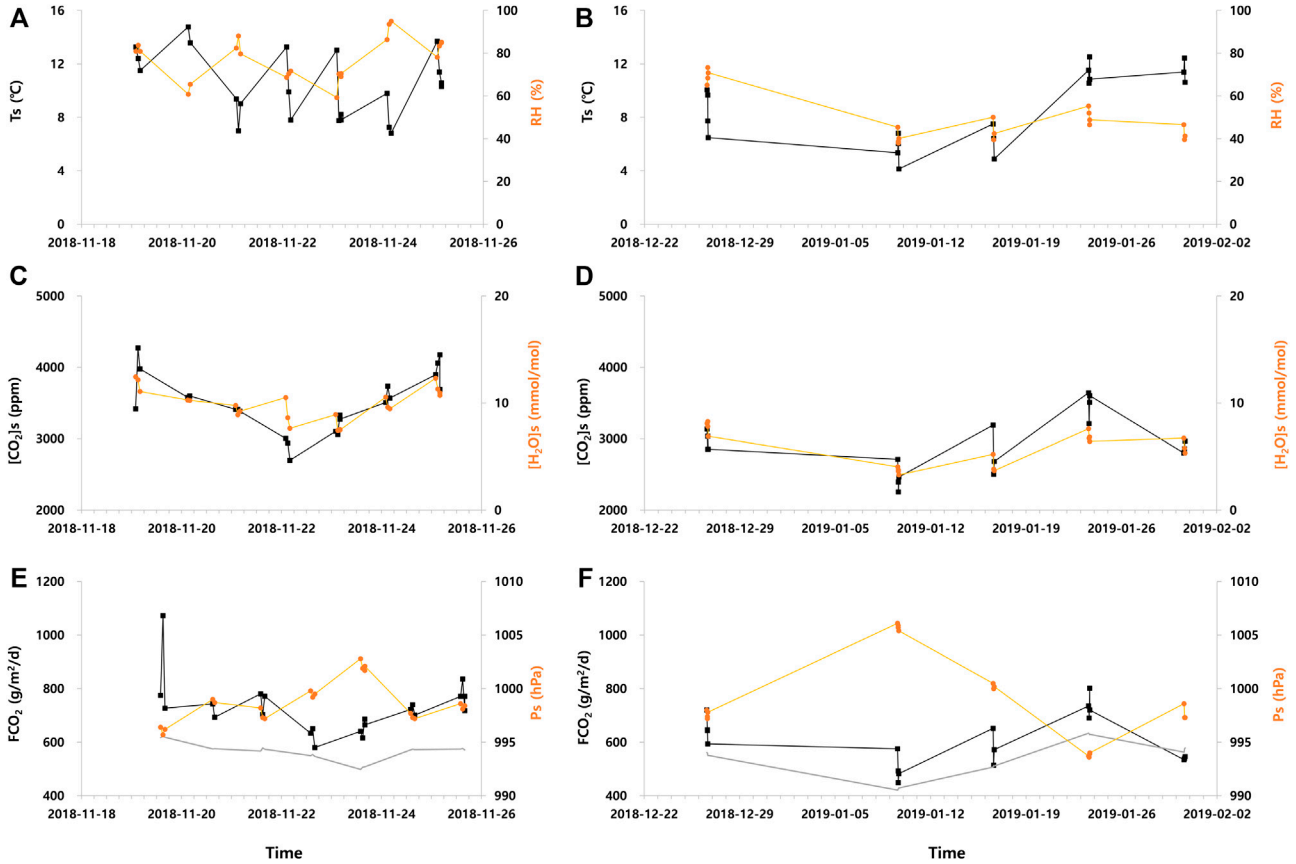

FIGURE 7 | Temporal comparison of temperature (Ts), relative humidity (RHs) in **(A,B)**, CO_2 concentrations ([CO_2]s), water vapor mole fraction ([H_2O]s) In **(C,D)**, and pressure (Ps) in the chamber and calculated CO_2 flux (FCO_2) In **(E,F)** during the period **II**. In **(E,F)** the gray line addresses the FCO_2 estimated using Taws and Paws in **Equation 3**. Note that the left (until November 25, 2018) and right figures (after December 26, 2018) have different scales of the x axis (time).

TABLE 5 | Pearson correlation coefficients during the period **II**. Absolute values ≥0.6 are in bold.

	FCO_2	T_s	RH_s	$[H_2O]_s$	$[CO_2]_s$	P_s	P_{aws}	T_{aws}	RH_{aws}	WS_1	WS_{10}	$[N_2]_v$	$[O_2]_v$	$[CO_2]_v$	$\delta^{13}C_{[CO2]v}$
FCO_2	1.0														
T_s	0.5	1.0													
RH_s	**0.7**	0.2	1.0												
$[H_2O]_s$	**0.8**	**0.7**	**0.8**	1.0											
$[CO_2]_s$	**0.9**	**0.6**	**0.7**	**0.8**	1.0										
P_s	**−0.6**	−0.5	−0.3	−0.5	**−0.6**	1.0									
P_{aws}	**−0.6**	**−0.6**	−0.4	−0.5	**−0.6**	**1.0**	1.0								
T_{aws}	**0.7**	**0.8**	0.4	**0.8**	**0.7**	**−0.6**	**−0.6**	1.0							
RH_{aws}	0.4	−0.1	**0.7**	0.5	0.5	−0.3	−0.3	0.1	1.0						
WS_1	−0.1	0.2	−0.3	−0.1	−0.2	−0.3	−0.3	0.0	−0.4	1.0					
WS_{10}	−0.1	0.0	−0.4	−0.3	−0.3	−0.2	−0.2	−0.1	−0.4	**0.8**	1.0				
$[N_2]_v$	0.4	**0.7**	**0.7**	**0.8**	0.4	−0.2	−0.3	**0.7**	0.4	−0.2	−0.1	1.0			
$[O_2]_v$	0.5	**0.6**	**0.7**	**0.8**	0.4	−0.1	−0.2	**0.6**	0.4	−0.2	−0.1	**1.0**	1.0		
$[CO_2]_v$	−0.5	**−0.6**	**−0.7**	**−0.8**	−0.4	0.1	0.1	**−0.6**	−0.3	0.2	0.1	**−0.9**	**−1.0**	1.0	
$\delta^{13}C_{[CO2]v}$	−0.5	−0.2	−0.4	−0.5	−0.2	0.2	0.3	−0.4	0.0	0.0	0.2	−0.3	−0.4	0.3	1.0

The impact of pressure variation on degassing was quantitatively compared to that of temperature and salinity in **Table 6** because the saline fluid in the deep part can rise temperature and salinity as well as pressure of groundwater. The salinity was assumed to be low (100–150 mg/L) because the CO_2-rich water in the study area was characterized by low pH and electrical conductivity (EC), probably due to short (<35 years) reaction times between water and rocks despite a large amount of CO_2 inflow into the aquifer (Kim et al., 2008; Chae et al., 2016). According to Chae et al. (2016), the

TABLE 6 | Sensitivity analysis of CO_2 degassing from a CO_2-rich water.

Scenario	T(°C)	T (K)	P (bar)	cNaCl (m)	mCO_2(m)
Base case	13	286.15	1	0.002[a]	0.0471
Increase in temperature	15	288.15	1	0.002[a]	0.0442
Increase in pressure	13	286.15	8.14[b]	0.002[a]	0.3692
Increase in salinity	13	286.15	1	0.003[c]	0.0471
Increase in all[d]	15	288.15	8.14[b]	0.003[c]	0.3474

[a]*Corresponding to the total dissolved solids (TDS) of 100 mg/L.*
[b]*At a depth of 80 m (w-2 in Figure 1A).*
[c]*Corresponding to TDS of 150 mg/L.*
[d]*The saline fluid in the deep part can rise temperature, pressure and salinity of groundwater altogether.*

temperature and salinity (EC) of the CO_2-rich water from w-2 varied between 11.6 and 15.8°C and between 108 and 175 μS/cm for 14 months, respectively. **Table 6** shows that the change in CO_2 solubility (i.e., degassing) is more influential by the pressure variation than by the temperature or salinity in the study site.

When the water is pumped and thus the water pressure drops, gas bubbles occurs in CO_2-rich water. Subsequently the gas release ceases and the gas dissolved in the CO_2-rich water is being released as a result of a slow diffusion process (Kouznetsov et al., 2002). The "bubbly" stage may be resumed at shaking (see *Possible Causes of a High CO_2 Emission During the Period* II*).* The changes in the water table also affect FCO_2 in the vadose zone as in Schroder et al. (2017) who found the FCO_2 distribution shifted between two CO_2 release tests due to the changes in groundwater depth in wet and dry season. The low water table in dry season facilitates lateral CO_2 migration, reducing FCO_2 along a wellbore. The quantitative assessment of the effect of pressure variation caused by water usage on the CO_2 degassing (and subsequently on FCO_2) in the study area remains future work due to little information on the water table and the amount of water consumption at w-2.

In addition, Chae et al. (2016) speculated dry CO_2 flowing directly into the aquifer of w-2 (80 m depth) from the magmatic origin, since the study site is located at the geologic boundary between gneiss and granite (**Figure 1A**) and unknown fractures may exist around the study area given the small earthquakes (**Figure 1B**) and CO_2-rich waters (**Supplementary Figure S1**), although none has been reported within 13 km around the study area. According to Kerrick and Caldeira (1998), the plutonic-metamorphic belt can be a source area to emit CO_2 to the atmosphere. In fact, Yu et al. (2015) observed the temporal variation of CO_2 supply to the aquifer for 48 h in a CO_2-rich spring (s-2 in **Figure 1A**), which decreased pH and increased total dissolved inorganic carbon (TDIC) and $\delta^{13}C_{TDIC}$ and might further cause the temporal variation of $[CO_2]_v$, $[CO_2]_s$, or FCO_2.

Environmental Parameters

We found the significant influence of air temperature (T_{aws}, T_s) and pressure (P_{aws}, P_s) to FCO_2 at all periods as the previous studies (Chiodini et al., 1998; Granieri et al., 2003; Carapezza et al., 2011; Camarda et al., 2016; Morita et al., 2019). The temperature was correlated with FCO_2 probably due to the effect of temperature to soil gas diffusivity near the M17 site, and not due to the biological effect in November (late fall during the period I) and December (winter during the period III) in South Korea (Camarda et al., 2016 and references therein). In particular, the high $[CO_2]_v$ at M17v during the period III suggested the accumulation of geogenic CO_2 in the subsurface due to low soil gas diffusion at cold weather.

T_s and P_s were highly related with T_{aws} and P_{aws} respectively ($r \geq 0.8$ at all periods), while RH_s was significantly with RH_{aws} ($r = 0.7$ at all periods) despite the 10 km distance of AWS from the study area. These high correlations between measurements imply the usefulness of the environmental data from the chamber in LI-COR and the AWS data. A multiple regression line using T_{aws} and P_{aws} for FCO_2 during the periods I and III was obtained respectively as:

$$FCO_2\_estimated\ for\ the\ period\ I = 2.8 \times T_{aws} - 14.8 \times P_{aws} + 15,752 \quad (3)$$

$$FCO_2\_estimated\ for\ the\ period\ III = 2.0 \times T_{aws} - 2.4 \times P_{aws} + 2,676 \quad (4)$$

which had $r^2 = 0.65$ and $p = 0.00$ in **Equation 3** and $r^2 = 0.53$ and $p = 0.00$ in **Equation 4**, supporting the significant effects of T_{aws} and P_{aws} to FCO_2. However, microclimates may greatly affect some environmental parameters. For instance, the wind speed (*WS*) from the AWS did not influence FCO_2 (**Tables 2**, **3**, **5**), probably because *WS*, which is sensitive to topography (Helbig et al., 2016), was not measured near the measurement point. **Table 4** shows the negative correlation of FCO_2 with *WS* at the time lag of −18 h. According to Carapezza et al. (2011), the negative effect of *WS* reflects that the gas is confined underground under strong wind conditions.

In addition to T_s and P_s, $[H_2O]_s$ (i.e., water vapor mole fraction in the chamber 2 min after closing the chamber), showed significant correlations with FCO_2 ($r \geq 0.5$) at all periods, while with $[CO_2]_s$ only during the period II ($r = 0.8$ in **Table 5**). $[H_2O]_s$ increased with T_s and T_{aws} but decreased with P_s and P_{aws} at all periods as FCO_2. Similarly, Schroder et al. (2016), Schroder et al. (2017) found some degree of spatial correlation between FCO_2 and surface H_2O fluxes and suggested that water vapor can be used as a proxy for escaping gas in some leak scenarios. Moreover, Schroder et al. (2016) discussed the possible source of the water, e.g., the same CO_2 reservoir or a function of the CO_2 passage through the water table, and proposed that the water is sourced from the same CO_2 reservoir based on the slightly elevated temperature of the upwelled water compared with surrounding groundwater in the Qinghai research site, whereas the CO_2 efflux transported H_2O from the top of the water table at or marginally above the release well at the Ginninderra controlled release facility, Australia (Schroder et al., 2017). Besides, Zhou et al. (2013) suggested that the released CO_2 not only depletes soil O_2 but also enhances evaporation and reduces the soil moisture.

On the other hand, the relative humidity (*RH*) was positively related with FCO_2 during the period II (e.g., $r = 0.7$ of RH_s and $r = 0.4$ of RH_{aws} in **Table 5**) but negatively with FCO_2 during the period I (**Table 2**), while not related with FCO_2 during the period III (**Table 3**). The different correlation between measurements suggests the different major mechanism for CO_2 transport, e.g., low gas diffusion at cold weather during the period III and the earthquake during the period II (see *Possible Causes of a High CO_2 Emission During the Period* II). Similarly, Zhou et al. (2013) found the opposite relationship between the soil O_2 concentration and soil moisture for the during-release and post-release due to the pumping effect of the released CO_2 gas plume at the interface between the CO_2 plume and the soil liquid water. Besides, the period II had precipitation. The precipitation may cause the CO_2 gas uprising, filling the pore with water (e.g., Lewicki et al., 2010; Johnson and Rostron, 2012; Garcia-Anton et al., 2014), although the opposite effect of precipitation is also possible, dissolving the CO_2 gas in infiltrating water (Annunziatellis et al., 2008) or reducing the gas permeability (e.g., Carapezza et al., 2011; Garcia-Anton et al., 2014).

Prevailing Mechanisms of CO_2 Transport

The high FCO_2 and its high correlation with P_{aws} indicate that the study site has a non-negligible advective component (Hernández et al., 2001; Ascione et al., 2018). Similarly, Kim et al. (2019) showed that the M17 site was located in the high-advection zone using the relationship between FCO_2 and $[CO_2]_s$ suggested by Jung et al. (2014). The negative correlation between P_{90} and $[CO_2]_v$ (**Table 2**) and the positive ΔP (1.0–1.3 hPa in **Table 1**; **Figure 3**) and thus the pressure gradient in the range of 1.1 and 1.4 hPa/m during the period I also suggest the advective flow upward in the unsaturated soil. Takle et al. (2004) showed that pressure differences between −15 and 15 Pa at depths of 0–60 cm caused FCO_2 exceeding diffusional fluxes due to pressure pumping. According to Altevogt and Celia (2004), the leakage rate of 0.1 g/m s to 100 g/m s were reached at a CO_2 source with the vertical pressure gradient of 0.18–49.65 hPa/m adjacent to the source boundary.

However, FCO_2 was affected by air temperature and $[H_2O]_s$ as well as air pressure in **Tables 2**, **3**, **5**, implying that the diffusive transport of CO_2 is also significant in the study site (Camarda et al., 2019). Accordingly, temperature gradient might affect the pressure gradient of 1.1 and 1.4 hPa/m during the period I, while the gradient was not measured. In addition, $[CO_2]_v$ showed different temporal changes from FCO_2 during the period I in **Figures 2E**, **4A** and its correlation with FCO_2 increased at the time lag of −16 h in **Table 4**. Moreover, soil CO_2 seems to mainly form through degassing of a CO_2-rich aquifer and the degassing may vary depending on the pressure variation in the aquifer for w-2 (**Table 6**).

Thus, it can be concluded that the advection is dominant at the near surface, while the transport of geogenic soil CO_2 is diffusive-dominated in the vadose zone by the CO_2 gradient. Similarly, Kim et al. (2018) observed that CO_2 concentrations measured at 15 cm depth were significantly lower than those measured at 60 cm depth, as the CO_2 gas escaped quickly into the atmosphere at the ground surface due to the atmospheric pressure effect at an inject test, for which approximately 1.8 t CO_2 was injected at 2.5 m depth with a CO_2 release rate of 6 L/min. Rillard et al. (2015) showed that the advective flux between an injection point and the surface through a preferential path was the dominant gas transport process during the injection phase because it was difficult to avoid a slight overpressure at the injection point. Altevogt and Celia (2004) determined the diffusive flux as well as the slip and Darcy fluxes associated with natural CO_2 leakage into the vadose zone based on a two-dimensional numerical model, and showed that the mole fraction-driven flux played an important role in the development of the CO_2 plume even in situations where pressure-driven advection was the dominant flux mechanism.

Heterogenous Transport of Geogenic CO_2

FCO_2 was in different ranges (**Table 1**) and had different correlations with measurements during the periods I and III (**Tables 2**, **3**) probably because the measurement points were not exactly the same but at the 30 cm separation between M17 (period I) and M17–1 (period III), implying the spatial variability of FCO_2, as reported by other researchers including Annunziatellis et al. (2008) and Ascione et al. (2018). Similar to this study result, Annunziatellis et al. (2008) mentioned a test showing a change of more than one order of magnitude over only 30 cm. However, the spatial difference in FCO_2 at the centimeter scale was not expected before the study area, and the extreme spatial variability of FCO_2 needs to be further studied in the study area.

Note that the different FCO_2 between November (period I) and December (period III) cannot be explained by the seasonal variation, given the similar FCO_2 between August (summer) in 2017 and November (fall) in 2018 despite distinct climate conditions. We acknowledge that the low FCO_2 might reflect the weather condition given the low temperature (T_s) and high pressure (P_s) during the period III (**Figure 2**) and their positive and negative influence on FCO_2 respectively (**Tables 2**, **3**). However, the different ranges in FCO_2 as well as in $[H_2O]_s$ and $[CO_2]_s$ between the periods I and III in **Figure 2** imply that the effect of heterogeneous CO_2 transport in the vadose zone is stronger than the weather effect. In addition, the FCO_2 estimated using **Equation 3** was much higher than the measured FCO_2 during the period III (**Supplementary Figure S6**).

Possible Causes of a High CO_2 Emission During the Period II

The FCO_2 value of 1,073 g/m^2/d was exceptionally high, exceeding the $\mu + 2\sigma$ of the period I (**Figure 6**). Besides, FCO_2 measurements were much higher than the estimations using **Equation 3**, in particular until November 25, 2018 (**Figures 7E,F**), implying the effect of factors other than T_{aws} and P_{aws}. Meanwhile, $[CO_2]_v$ rapidly decreased after the earthquake. This anomalously high FCO_2 peak and sudden decreases in $[CO_2]_v$ during the period II cannot be explained by the environmental parameters given similar climate conditions (**Table 1**), and imply a high CO_2 emission, causing that FCO_2 was negatively related with $[CO_2]_v$ ($r = -0.5$ in **Table 5**). In addition, $[CO_2]_s$ was highly correlated with FCO_2 ($r = 0.9$), and the residual FCO_2 filtered by T_{aws} and P_{aws} was also well correlated with $[CO_2]_s$

(**Supplementary Figure S7**; r = 0.7). According to Camarda et al. (2019), the relationship between FCO_2 and environmental parameters depends on the amount of deep CO_2 supply as well as the prevalent process of CO_2 transport. **Table 5** shows that the FCO_2 variations brought by $[CO_2]_s$, RH_s and RH_{aws} increased after the earthquake.

Emission Scenario

We suggest that vibrations caused by the earthquake induced the soil gas to transport to the surface, with rapidly decreasing $[CO_2]_v$ and increasing $[CO_2]_s$ and FCO_2 since the study site is located between the geologic boundary (**Figure 1**) and unknown fracture may exist, while CO_2 gas probably forms by degassing of a CO_2-rich aquifer and leaks through the well (w-2) casing in the shallow (<80 m) subsurface given no high flux except M17 near w-2. Earthquake might increase air permeability by a change in site features or modification of the structural parts of the well (w-2) from which the CO_2 originates. Besides, mechanical processes, including vibrations induced by an earthquake, have been known to increase degassing of dissolved gas and to enhance the movement of gas bubbles in fractured aquifers (Kouznetsov et al., 1998; Toutain and Baubron, 1999; Manga et al., 2012), changing the physicochemical parameters of water (e.g., EC, pH, temperature, water level). According to Kouznetsov et al. (1998), degassing is related to local instantaneous ruptures in the formation fluid due to the effect of elastic waves. Nuclei of bubbles are formed in these ruptures, and gas diffusion from fluid into these bubbles takes place (Kouznetsov et al., 1998). Crews and Cooper (2014) also showed that seismic waves initiated bubble nucleation and growth in groundwater, which increased the water level in boreholes, reducing effective stress in critically loaded geologic faults, and consequently induced secondary earthquakes. Fischer et al. (2017) observed the CO_2 bubbles increasing in a CO_2-rich well water 4 days after a 3.5 M earthquake occurring 9 km away. The high CO_2 bubble concentrations lasted for 150 days.

We acknowledge that it is difficult to determine whether the high FCO_2 and low $[CO_2]_v$ were caused by the earthquake because of the short-term and discontinuous data with only a small earthquake. Besides, this observation was opposite to the jumps of both FCO_2 and $[CO_2]_v$ in soil gas wells during the seismic activity in the active fault zones (Chen et al., 2020). We did not observe the CO_2-rich water to support the emission scenario during this study. However, the impact of the small earthquake cannot be excluded for the high FCO_2 during the period II, given that FCO_2 measured immediately after the earthquake was beyond the seasonal and diurnal variation of FCO_2 at M17 (**Table 1**) and much higher than that estimated using T_{aws} and P_{aws} (**Figure 7**). Moreover, it should be noted that we began to measure FCO_2 12 h after the earthquake occurred, and we might miss higher values given a synchronous sharp increase of seismicity and FCO_2 in a seismically active area (Camarda et al., 2016) and the velocity of P (7–8 km/s) and S wave (4–5 km/s).

Suggestion of an Earthquake Precursor

We noted that $[CO_2]_v$ rapidly increased to be 48.9% on 22:00 November 2, 2018, and then the maximum $[C\ O_2]_s$ was observed 12 h later (**Figures 2C**, **4A**), approximately 16 days before the earthquake (**Figure 6**). Besides, FCO_2 had an increasing trend during the period I (r^2 = 0.3 in **Figure 6**), although the average FCO_2 (564 g/m$_2$/d) was similar to 546 g/m^2/d obtained at M17 in August 2017 (**Table 1**). These temporal variations might be a precursor of the earthquake. We acknowledge that many researches have been carried out on the precursors of earthquakes, while there is no general agreement among scientists on the earthquake precursors (Tsunogai and Wakita, 1995; Hernández et al., 2001; Pérez et al., 2008; Ingebritsen and Manga, 2014). Besides, the changes in soil CO_2 have been reported as a result of earthquakes or volcanic activities, rather than an earthquake precursor (Hernández et al., 2001; Troll et al., 2012). Moreover, only one earthquake case was observed in this study (**Supplementary Figure S2**).

However, many studies suggested the soil gas to be one of the most reliable tools to investigate earthquake precursory signals (Walia et al., 2010; Sciarra et al., 2017). For instance, Sciarra et al. (2017) suggested that crustal dilation linked to seismic activity favors the uprising of geogas toward the surface. Walia et al. (2010) showed that the spatial distribution of soil gases was useful in identifying tectonic systems since it showed a clear anomalous trend along the Hsinhua Fault. Chiodini et al. (2004) found in the Apennine that the anomalous FCO_2 suddenly disappeared in a narrow band with the seismicity concentrated, and suggested that the gas accumulates in crustal traps at depth, generating CO_2 overpressurized reservoirs, which induce seismicity.

CONCLUSION

Temporal variations of soil CO_2 flux (FCO_2) and soil CO_2 concentration ($[CO_2]_v$) were investigated for three periods to recognize the factors controlling the temporal variation of geogenic FCO_2 in a non-volcanic and seismically inactive area. The periods I (November 2 to 5, 2018) and III (December 2 to 8, 2019) were to assess the baseline, while the period II (November 19, 2018 to January 30, 2019) was to survey the effect of a small (2.1 M) earthquake occurring 7.8 km away. The correlation coefficients indicated that the air pressure was the most significant controlling factor to FCO_2 regardless of the periods, and the air temperature was also noteworthy.

In contrast, some environmental parameters were significantly related with FCO_2 during one or two periods only, e.g., $[CO_2]_s$ and $[CO_2]_v$ during the period II. In particular, the low $[CO_2]_v$ but high FCO_2 during the period II implied the high emission of soil CO_2 after the small earthquake, which affected the relations between some environmental parameters (e.g., $[CO_2]_s$, RH_s and RH_{aw}) and FCO_2. Meanwhile, the low FCO_2 during the period III suggested the heterogenous subsurface conditions for CO_2 transport at the centimeter scale, while the high $[CO_2]_v$ implied the accumulation of soil CO_2 in the subsurface due to low soil gas diffusion at cold weather. Based on the high FCO_2, its high correlation with air temperature as well as air pressure, and the different temporal changes of $[CO_2]_v$ from FCO_2 including the high $[CO_2]_v$ at cold weather, the study area seemed to have the diffusive transport of soil CO_2 dominant in the vadose zone, while the advection near the surface.

The merit of this study is to present the temporal variation of high FCO_2 of deep CO_2 origin in a non-volcanic and seismically inactive area and to discuss the controlling factors, given few studies on the temporal changes of geogenic CO_2 emissions in a geologically

stable region, although CO_2-rich water discharges. In particular, we found a rapid increase of FCO_2 after the small earthquake, which implies that the global natural CO_2 emission can be larger than the previous estimation. In addition, artificial vibrations (e.g., building construction and transportation vibration) may enhance natural CO_2 emissions, and thus CO_2-rich waters or FCO_2 should be monitored to assess the effect of artificial and natural vibrations to CO_2 emissions. Besides, we provided the usefulness of data in the chamber and AWS data to understand the temporal variation in FCO_2.

We acknowledge however that we only observed a period (II) with respect to an earthquake because the study area has low and sporadic seismicity and no automated FCO_2 monitoring system. It was difficult to determine a cause for the high FCO_2 peak and decreases in $[CO_2]_v$ mostly because of short-term and discontinuous monitoring at different acquisition intervals. Thus our speculation about the effect of the small earthquake to abnormal increases in FCO_2 and the applicability of $[CO_2]_v$ as an earthquake precursor needs to be confirmed through a physics-based numerical modeling work and long-term monitoring data. A process-based understanding for the effects of earthquakes to FCO_2 and $[CO_2]_v$ remains future work. Besides, we could not clearly explain the irregular temporal variations of $[CO_2]_s$ and its high correlation with FCO_2 during the period II. Thus, the carbon isotopic compositions of $[CO_2]_s$ is also needed to be investigated in the next study. With defining end-member properties, the proportion of geogenic CO_2 in $[CO_2]_s$ should be assessed to verify the temporal variation of geogenic CO_2 supply with $[CO_2]_s$. Lastly, the low FCO_2 during the period III implied the high spatial variability of FCO_2. A spatially intensive FCO_2 investigation close to M17 will be conducted in the near future to address the reason for heterogeneity in the centimeter scale.

Based on the temporal changes in FCO_2 in this non-volcanic and seismically inactive study area, we suggest to install an automated FCO_2 monitoring system in natural emission sites to understand temporal increases in natural CO_2 emissions and their causes (e.g., earthquake) in geologically stable regions and consequently the global natural CO_2 emission based on long-term monitoring data. In particular, the FCO_2 monitoring should be complemented with the monitoring of degassing from groundwater to assess the impact of tectonic stresses because endogenous factors affect the physicochemical parameters of water as well, which subsequently changes CO_2 concentrations and FCO_2.

DATA AVAILABILITY STATEMENT

The datasets presented in this study can be found in online repositories. The names of the repository/repositories and accession number(s) can be found below: https://zenodo.org/record/3818108#.X0c3DOR7k6Y.

AUTHOR CONTRIBUTIONS

CK conducted the field work, wrote a first draft, and made figures. SY interpreted the data, wrote the manuscript, and made figures. Y-YO interpreted the temporal data and suggested the cross-correlation analysis. GC designed and initiated the field work, and acquired and interpreted the data. S-TY contributed to the conception and design of the work. YS supervised the field work and sample analysis. All authors contributed to discussions and revisions of the manuscript.

FUNDING

This research was supported by the fundamental research project of KIGAM (Korea Institute of Geoscience and Mineral resources) and was partially supported by the National Research Foundation of Korea (NRF) grant funded by the Korean government (MEST) (No. 2019R1A2C1084297) and the Korea Ministry of Environment (MOE) as K-COSEM (Korea CO_2 Storage Environmental Management) Research Program.

ACKNOWLEDGMENTS

The authors acknowledge diligent field and laboratory works by Inhye Lee, Byeongjun Park, and Gibeom Seok.

SUPPLEMENTARY MATERIAL

The Supplementary Material for this article can be found online at: https://www.frontiersin.org/articles/10.3389/feart.2020.599388/full#supplementary-material.

REFERENCES

Altevogt, A. S., and Celia, M. A. (2004). Numerical modeling of carbon dioxide in unsaturated soils due to deep subsurface leakage. *Water Resour. Res.* 40, W03509. doi:10.1029/2003WR002848

Annunziatellis, A., Beaubien, S. E., Bigi, S., Ciotoli, G., Coltella, M., and Lombardi, S. (2008). Gas migration along fault systems and through the vadose zone in the Latera caldera (central Italy): implication for CO_2 geological storage. *Int. J. Greenhouse Gas Control* 2 (3), 353–372. doi:10.1016/j.ijggc.2008.02.003

Ascione, A., Ciotoli, G., Bigi, S., Buscher, J., Mazzoli, S., Ruggiero, L., et al. (2018). Assessing mantle versus crustal sources for non-volcanic degassing along fault zones in the actively extending southern Apennines mountain belt (Italy). *GSA Bulletin* 130 (9-10), 1697–1722. doi:10.1130/B31869.1

Auer, L. H., Rosenberg, N. D., Birdsell, K. H., and Whitney, E. M. (1996). The effects of barometric pumping on contaminant transport. *J. Contam. Hydrol.* 24 (2), 145–166. doi:10.1016/S0169-7722(96)00010-1

Baines, S. J., and Worden, R. H. (2004). The long-term fate of CO2 in the subsurface: natural analogues for CO2 storage. *Geol. Soc. London Spec. Publ.* 233 (1), 59–85. doi:10.1144/GSL.SP.2004.233.01.06

Burton, M. R., Sawyer, G. M., and Granieri, D. (2013). Deep carbon emissions from volcanoes. *Rev. Mineral. Geochem.* 75 (1), 323–354. doi:10.2138/rmg.2013.75.11

Camarda, M., De Gregorio, S., Di Martino, R. M., and Favara, R. (2016). Temporal and spatial correlations between soil CO_2 flux and crustal stress. *J. Geophys. Res. Solid Earth.* 121 (10), 7071–7085. doi:10.1002/2016JB013297

Camarda, M., De Gregorio, S., Capasso, G., Di Martino, R. M., Gurrieri, S., and Prano, V. (2019). The monitoring of natural soil CO_2 emissions: issues and

perspectives. *Earth Sci. Rev.* 198, 102928. doi:10.1016/j.earscirev.2019.102928

Carapezza, M. L., Barberi, F., Ranaldi, M., Ricci, T., Tarchini, L., Barrancos, J., et al. (2011). Diffuse CO_2 soil degassing and CO_2 and H_2S concentrations in air and related hazards at vulcano island (aeolian arc, italy). *J. Volcanol. Geoth. Res.* 207 (3-4), 130–144. doi:10.1016/j.jvolgeores.2011.06.010

Cardellini, C., Chiodini, G., and Frondini, F. (2003). Application of stochastic simulation to CO2 flux from soil: mapping and quantification of gas release. *J. Geophys. Res. Solid Earth* 108 (B9), 2425. doi:10.1029/2002JB002165

Chae, G., Yu, S., Jo, M., Choi, B. Y., Kim, T., Koh, D. C., et al. (2016). Monitoring of CO_2-rich waters with low pH and low EC: an analogue study of CO_2 leakage into shallow aquifers. *Environ. Earth Sci.* 75 (5), 390. doi:10.1007/s12665-015-5206-9

Chen, Z., Li, Y., Martinelli, G., Liu, Z., Lu, C., and Zhao, Y. (2020). Spatial and temporal variations of CO_2 emissions from the active fault zones in the capital area of china. *Appl. Geochem.* 112, 104489. doi:10.1016/j.apgeochem.2019.104489

Chiodini, G., Cardellini, C., Amato, A., Boschi, E., Caliro, S., Frondini, F., et al. (2004). Carbon dioxide earth degassing and seismogenesis in central and southern italy. *Geophys. Res. Lett.* 31 (7), L07615. doi:10.1029/2004GL019480

Chiodini, G., Cioni, R., Guidi, M., Raco, B., and Marini, L. (1998). Soil CO_2 flux measurements in volcanic and geothermal areas. *Appl. Geochem.* 13 (5), 543–552. doi:10.1016/S0883-2927(97)00076-0

Chiodini, G., Frondini, F., Kerrick, D. M., Rogie, J., Parello, F., Peruzzi, L., et al. (1999). Quantification of deep CO_2 fluxes from Central Italy. Examples of carbon balance for regional aquifers and of soil diffuse degassing. *Chem. Geol.* 159 (1-4), 205–222. doi:10.1016/S0009-2541(99)00030-3

Chiodini, G., Frondini, F., Cardellini, C., Granieri, D., Marini, L., and Ventura, G. (2001). CO_2 degassing and energy release at solfatara volcano, campi flegrei, italy. *J. Geophys. Res. Solid Earth* 106 (B8), 16213–16221. doi:10.1029/2001JB000246

Chiodini, G., Granieri, D., Avino, R., Caliro, S., Costa, A., and Werner, C. (2005). Carbon dioxide diffuse degassing and estimation of heat release from volcanic and hydrothermal systems. *J. Geophys. Res. Solid Earth* 110 (B8), B08204. doi:10.1029/2004JB003542

Ciotoli, G., Bigi, S., Tartarello, C., Sacco, P., Lombardi, S., Ascione, A., et al. (2014). Soil gas distribution in the main coseismic surface rupture zone of the 1980, M_s= 6.9, Irpinia earthquake (southern italy). *J. Geophys. Res. Solid Earth* 119 (3), 2440–2461. doi:10.1002/2013JB010508

Ciotoli, G., Etiope, G., Marra, F., Florindo, F., Giraudi, C., and Ruggiero, L. (2016). Tiber delta CO2-CH4 degassing: a possible hybrid, tectonically active Sediment-Hosted Geothermal system near rome. *J. Geophys. Res. Solid Earth* 121 (1), 48–69. doi:10.1002/2015JB012557

Crews, J. B., and Cooper, C. A. (2014). Experimental evidence for seismically initiated gas bubble nucleation and growth in groundwater as a mechanism for coseismic borehole water level rise and remotely triggered seismicity. *J. Geophys. Res. Solid Earth* 119 (9), 7079–7091. doi:doi.org/10.1002/2014JB011398

Duan, Z., and Sun, R. (2003). An improved model calculating CO_2 solubility in pure water and aqueous NaCl solutions from 273 to 533 K and from 0 to 2000 bar. *Chem. Geol.* 193 (3-4), 257–271. doi:10.1016/S0009-2541(02)00263-2

Faure, G. (1998). *Principles and applications of geochemistry*. Upper Saddle River, New Jersey: Prentice-Hall, Vol. 625.

Fischer, T., Matyska, C., and Heinicke, J. (2017). Earthquake-enhanced permeability–evidence from carbon dioxide release following the ML 3.5 earthquake in West bohemia. *Earth Planet Sci. Lett.* 460, 60–67. doi:10.1016/j.epsl.2016.12.001

Fischer, T. P., Arellano, S., Carn, S., Aiuppa, A., Galle, B., Allard, P., et al. (2019). The emissions of CO_2 and other volatiles from the world's subaerial volcanoes. *Sci. Rep.* 9, 18716. doi:10.1038/s41598-019-54682-1

Garcia-Anton, E., Cuezva, S., Fernandez-Cortes, A., Benavente, D., and Sanchez-Moral, S. (2014). Main drivers of diffusive and advective processes of CO_2-gas exchange between a shallow vadose zone and the atmosphere. *Int. J. Greenh. Gas Con.* 21, 113–129.

Granieri, D., Chiodini, G., Marzocchi, W., and Avino, R. (2003). Continuous monitoring of CO_2 soil diffuse degassing at phlegraean fields (Italy): influence of environmental and volcanic parameters. *Earth Planet Sci. Lett.* 212, 167–179. doi:10.1016/s0012-821x(03)00232-2

Helbig, N., Mott, R., van Herwijnen, A., Winstral, A., and Jonas, T. (2016). Parameterizing surface wind speed over complex topography. *JGR Atmosphere* 122 (2), 651–667. doi:10.1002/2016jd025593

Hernández, P. A., Salazar, J. M., Shimoike, Y., Mori, T., Notsu, K., and Pérez, N. (2001). Diffuse emission of CO2 from miyakejima volcano, japan. *Chem. Geol.* 177 (1-2), 175–185. doi:10.1016/S0009-2541(00)00390-9

Ingebritsen, S. E., and Manga, M. (2014). Earthquakes: hydrogeochemical precursors. *Nat. Geosci.* 7 (10), 697–698. doi:10.1038/ngeo2261

Jeong, C. H., Kim, H. J., and Lee, S. Y. (2005). Hydrochemistry and genesis of CO_2-rich springs from mesozoic granitoids and their adjacent rocks in south korea. *Geochem. J.* 39 (6), 517–530. doi:10.2343/geochemj.39.517

Jeong, C. H., Kim, J. G., and Lee, J. Y. (2001). Occurrence, geochemistry and origin of CO_2-rich water from the chungcheong area, korea. *Econo. Environ. Geol.* 34, 227–241. doi:10.9720/kseg.2016.4.515

Johnson, J. W., and Rostron, B. J. (2012). "Geochemical monitoring," in Best practices for validating CO_2 geological storage: observations and guidance from the IEAGHG Weyburn-Midale CO_2 monitoring and storage project. *Editor B. Hitchon (Alberta, Canada: Geoscience Pub.)* 119–154.

Jung, N. H., Han, W. S., Watson, Z. T., Graham, J. P., and Kim, K. Y. (2014). Fault-controlled CO_2 leakage from natural reservoirs in the colorado plateau, east-central utah. *Earth Planet Sci. Lett.* 403, 358–367. doi:10.1016/j.epsl.2014.07.012

Kerrick, D. M., and Caldeira, K. (1994). Metamorphic CO_2 degassing and early cenozoic paleoclimate. *GSA Today* 4 (3), 57–65.

Kerrick, D. M., and Caldeira, K. (1998). Metamorphic CO_2 degassing from orogenic belts. *Chem. Geol.* 145 (3-4), 213–232. doi:10.1016/S0009-2541(97)00144-7

Kerrick, D. M., and Caldeira, K. (1993). Paleoatmospheric consequences of CO_2 released during early Cenozoic regional metamorphism in the Tethyan orogen. *Chem. Geol.* 108 (1-4), 201–230. doi:10.1016/0009-2541(93)90325-D

Kerrick, D. M., McKibben, M. A., Seward, T. M., and Caldeira, K. (1995). Convective hydrothermal CO_2 emission from high heat flow regions. *Chem. Geol.* 121 (1-4), 285–293. doi:10.1016/0009-2541(94)00148-2

Kihm, Y. H., and Kim, J. H. (2003). Structural characteristics of the central Ogcheon Belt, South Korea: orogen-parallel tectonic transport model. *J. Asian Earth Sci.* 22, 41–57. doi:10.1016/s1367-9120(03)00022-1

Kim, H.-J., Han, S. H., Kim, S., Yun, S.-T., Jun, S.-C., Oh, Y.-Y., et al. (2018). Characterizing the spatial distribution of CO_2 leakage from the shallow CO_2 release experiment in south korea. *Int. J. Greenhouse Gas Control* 72, 152–162.

Kim, J., Yu, S., Yun, S. T., Kim, K. H., Kim, J. H., Shinn, Y. J., et al. (2019). CO_2 leakage detection in the near-surface above natural CO_2-rich water aquifer using soil gas monitoring. *Int. J. Greenhouse Gas Control* 88, 261–271. doi:10.1016/j.ijggc.2019.06.015

Kim, K., Jeong, D. H., Kim, Y., Koh, Y. K., Kim, S. H., and Park, E. (2008). The geochemical evolution of very dilute CO_2-rich water in Chungcheong Province, Korea: processes and pathways. *Geofluids* 8 (1), 3–15. doi:10.1111/j.1468-8123.2007.00200.x

KMA (Korea Meteorological Administration) (2019). Weather information. Available at: https://www.weather.go.kr.

Kouznetsov, O. L., Simkin, E. M., Chilingar, G. V., and Katz, S. A. (1998). Improved oil recovery by application of vibro-energy to waterflooded sandstones. *J. Petrol. Sci. Eng.* 19 (3-4), 191–200. doi:10.1016/S0920-4105(97)00022-3

Kouznetsov, O. L., Simkin, E. M., Chilingar, G. V., Gorfunkel, M. V., and Robertson, J. O. (2002). Seismic techniques of enhanced oil recovery: experimental and field results. *Energy Sources* 24 (9), 877–889. doi:10.1080/00908310290086761

Lewicki, J. L., Hilley, G. E., Dobeck, L., and Spangler, L. (2010). Dynamics of CO2 fluxes and concentrations during a shallow subsurface CO2 release. *Environ. Earth Sci.* 60, 285–297.

Lee, H., Muirhead, J. D., Fischer, T. P., Ebinger, C. J., Kattenhorn, S. A., Sharp, Z. D., et al. (2016). Massive and prolonged deep carbon emissions associated with continental rifting. *Nat. Geosci.* 9, 145–149. doi:10.1038/ngeo2622

Lewicki, J. L., Hilley, G. E., Dobeck, L., and Spangler, L. (2010). Dynamics of CO_2 fluxes and concentrations during a shallow subsurface CO_2 release. *Environ. Earth Sci.* 60, 285–297.

Manga, M., Beresnev, I., Brodsky, E. E., Elkhoury, J. E., Elsworth, D., Ingebritsen, S. E., et al. (2012). Changes in permeability caused by transient stresses: field observations, experiments, and mechanisms. *Rev. Geophys.* 50 (2), RG2004. doi:10.1029/2011RG000382

Massmann, J., and Farrier, D. F. (1992). Effects of atmospheric pressures on gas transport in the vadose zone. *Water Resour. Res.* 28 (3), 777–791. doi:10.1029/91WR02766

MCT (Ministry of Construction and Transportation), KRCC (Korea Rural Community Co.), and K–Water. (2006). Groundwater basic survey in the Yeongi area. No. 11–1500000–01811–01.

Morita, M., Mori, T., Yokoo, A., Ohkura, T., and Morita, Y. (2019). Continuous monitoring of soil CO 2 flux at aso volcano, japan: the influence of environmental parameters on diffuse degassing. *Earth Planets Space* 71 (1), 1. doi:10.1186/s40623-018-0980-8

Mörner, N. A., and Etiope, G. (2002). Carbon degassing from the lithosphere. *Global Planet. Change* 33 (1-2), 185–203. doi:10.1016/S0921-8181(02)00070-X

Oliveira, S., Viveiros, F., Silva, C., and Pacheco, J. E. (2018). Automatic filtering of soil CO2 flux data; different statistical approaches applied to long time series. *Front. Earth Sci.* 6, 208. doi:10.3389/feart.2018.00208

Pérez, N. M., Hernández, P. A., Igarashi, G., Trujillo, I., Nakai, S., Sumino, H., et al. (2008). Searching and detecting earthquake geochemical precursors in CO_2-rich groundwaters from galicia, spain. *Geochem. J.* 42 (1), 75–83. doi:10.2343/geochemj.42.75

R core team (2019). *R: a language and environment for statistical computing*. Vienna, Austria: R Foundation for Statistical Computing.

Ricci, T., Finizola, A., Barde-Cabusson, S., Delcher, E., Alparone, S., Gambino, S., et al. (2015). Hydrothermal fluid flow disruptions evidenced by subsurface changes in heat transfer modality: the la fossa cone of vulcano (Italy) case study. *Geology* 43 (11), 959–962. doi:10.1130/G37015.1

Rillard, J., Loisy, C., Le Roux, O., Cerepi, A., Garcia, B., Noirez, S., et al. (2015). The DEMO-CO2 project: a vadose zone CO2 and tracer leakage field experiment. *Int. J. Greenhouse Gas Control* 39, 302–317. doi:10.1016/j.ijggc.2015.04.012

Rogie, J. D., Kerrick, D. M., and Sorey, M. L. (2001). Dynamics of carbon dioxide emission at mammoth mountain, california. *Earth Planet Sci. Lett.* 188, 535–541. doi:10.1016/s0012-821x(01)00344-2

Romanak, K. D., Bennett, P. C., Yang, C., and Hovorka, S. D. (2012). Process-based approach to CO_2 leakage detection by vadose zone gas monitoring at geologic CO_2 storage sites. *Geophys. Res. Lett.* 39 (15), L15405. doi:10.1029/2012GL052426

Sano, Y., and Marty, B. (1995). Origin of carbon in fumarolic gas from island arcs. *Chem. Geol.* 119 (1–4), 265–274. doi:10.1016/0009-2541(94)00097-R

Schroder, I. F., Zhang, H., Zhang, C., and Feitz, A. J. (2016). The role of soil flux and soil gas monitoring in the characterisation of a CO_2 surface leak: a case study in qinghai, china. *Int. J. Greenhouse Gas Control* 54, 84–95. doi:10.1016/j.ijggc.2016.07.030

Schroder, I. F., Wilson, P., Feitz, A. F., and Ennis-King, J. (2017). Evaluating the performance of soil flux surveys and inversion methods for quantification of CO2 leakage. *Energy Procedia* 114, 3679–3694. doi:10.1016/j.egypro.2017.03.1499

Sciarra, A., Cantucci, B., and Coltorti, M. (2017). Learning from soil gas change and isotopic signatures during 2012 emilia seismic sequence. *Sci. Rep.* 7 (1), 1–7. doi:10.1038/s41598-017-14500-y

Sun, Y., Guo, Z., Liu, J., and Du, J. (2018). CO_2 diffuse emission from maar lake: an example in changbai volcanic field, NE china. *J. Volcanol. Geoth. Res.* 349, 146–162. doi:10.1016/j.jvolgeores.2017.10.012

Takle, E. S., Massman, W. J., Brandle, J. R., Schmidt, R. A., Zhou, X., Litvina, I. V., et al. (2004). Influence of high-frequency ambient pressure pumping on carbon dioxide efflux from soil. *Agric. For. Meteorol.* 124, 193–206. doi:10.1016/j.agrformet.2004.01.014

Toutain, J. P., and Baubron, J. C. (1999). Gas geochemistry and seismotectonics: a review. *Tectonophysics* 304 (1-2), 1–27. doi:10.1016/S0040-1951(98)00295-9

Troll, V. R., Hilton, D. R., Jolis, E. M., Chadwick, J. P., Blythe, L. S., Deegan, F. M., et al. (2012). Crustal CO_2 liberation during the 2006 eruption and earthquake events at Merapi volcano, indonesia. *Geophys. Res. Lett.* 39 (11), L11302. doi:10.1029/2012GL051307

Tsunogai, U., and Wakita, H. (1995). Precursory chemical changes in ground water: kobe earthquake, japan. *Science* 269 (5220), 61–63. doi:10.1126/science.269.5220.61

Vodnik, D., Videmšek, U., Pintar, M., Maček, I., and Pfanz, H. (2009). The characteristics of soil CO_2 fluxes at a site with natural CO_2 enrichment. *Geoderma* 150 (1-2), 32–37. doi:10.1016/j.geoderma.2009.01.005

Walia, V., Lin, S. J., Fu, C. C., Yang, T. F., Hong, W. L., Wen, K. L., et al. (2010). Soil–gas monitoring: a tool for fault delineation studies along hsinhua fault (Tainan), southern taiwan. *Appl. Geochem.* 25 (4), 602–607. doi:10.1016/j.apgeochem.2010.01.017

White, F. M., and Corfield, I. (2006). *Viscous fluid flow*. New York: McGraw-Hill, Vol. 3, 433–434.

Woo, J. U., Rhie, J., Kim, S., Kang, T. S., Kim, K. H., and Kim, Y. (2019). The 2016 Gyeongju earthquake sequence revisited: aftershock interactions within a complex fault system. *Geophys. J. Int.* 217 (1), 58–74. doi:10.1093/gji/ggz009

Yu, S., Chae, G., Jo, M., Kim, J. C., and Yun, S. T. (2015). *Assessment of CO2 discharge in a spring using time-variant stable carbon isotope data as a natural analogue study of CO2 leakage*. Vienna, Austria: EGU general assembly, Vol. 17.

Zhou, X., Apple, M. E., Dobeck, L. M., Cunningham, A. B., and Spanglerc, L. H. (2013). Observed response of soil O_2 concentration to leaked CO_2 from an engineered CO_2 leakage experiment. *Int. J. Greenh. Gas Con.* 16, 116–128.

Zhu, M., Xue, W., Xu, H., Gao, Y., Chen, S., Li, B., et al. (2019). Diurnal and seasonal variations in soil respiration of four plantation forests in an urban park. *Forests* 10 (6), 513. doi:10.3390/f10060513

Conflict of Interest: The authors declare that the research was conducted in the absence of any commercial or financial relationships that could be construed as a potential conflict of interest.